Surface Properties of Crandallite in Relation to Froth Flotation

by

Sarthak Kaushik

B.Tech Mineral Engineering, Indian School of Mines, 2009

A THESIS SUBMITTED IN PARTIAL FULFILLMENT OF
THE REQUIREMENTS FOR THE DEGREE OF

MASTER OF APPLIED SCIENCE

in

The Faculty of Graduate Studies

(Mining Engineering)

THE UNIVERSITY OF BRITISH COLUMBIA

(Vancouver)

June 2012

© Sarthak Kaushik 2012

Abstract

The surface properties of crandallite relevant to the anionic flotation of salt-type minerals were investigated through electrokinetic, turbidity, and wettability techniques. All the tests were performed on fine crandallite particles as a function of pH and reagent concentration. The selected reagents included starch and oleic acid.

From the zeta potential measurements, the iso-electric point of crandallite was found to be at pH 5.5 and the mineral surface can be expected to be negatively charged under typical flotation conditions (pH 9-11). The value of the iso-electric point correlated well with the stability of crandallite particles towards aggregation. Suspensions of fine crandallite showed minimum turbidity at pH 5.5 suggesting that the aggregation of the mineral was most pronounced at the iso-electric point. Calcium ions behaved as potential determining ions by increasing the iso-electric point to pH 6.5. In addition, calcium ions also acted as specifically adsorbing ions at higher pH.

In the presence of starch, crandallite particles were strongly flocculated producing supernatants with the clarity of tap water. At the same time, the effect of starch on the zeta potential of crandallite was rather weak, consistent with the non-ionic character of the polysaccharide. The stability of crandallite towards aggregation was not strongly affected by oleic acid suggesting that the surfactant did not interact with the mineral. Wettability measurements on crandallite particles showed that oleic acid did not render the mineral particles hydrophobic at pH 10.5 (under normal flotation conditions) or at pH 7, which was in strong contrast to the wettability response of apatite. Under these conditions, crandallite surface was negatively charged and the adsorption of the anionic surfactant seemed to involve physical electrostatic forces as opposed to chemical interactions known to occur between apatite and oleic acid.

Overall, the experimental results strongly suggest that crandallite remains

hydrophilic during apatite flotation at pH 10.5 and the main mechanism of contamination of apatite concentrates by crandallite is through mechanical entrainment in the froth rather than by true flotation. In this respect, the role of starch as a flocculant should be beneficial in reducing the amount of fine crandallite reporting to the apatite concentrate.

Table of Contents

Appendices

List of Tables

List of Figures

Acknowledgments

I would like to express my deepest gratitude to my advisor, Dr. Marek Pawlik for his guidance, patience and providing me an excellent atmosphere for research. This thesis would not have been possible without his support and valuable comments. A sincere thank is also extended to the committee members.

I sincerely thank fellow graduate students in the department of Mining Engineering, particularly Mr. Jophat Engwayu and Mr. Esau Arinaitwe, for their patience and efforts in helping with the experimental setup and analysis techniques. I would also take this opportunity to thank Mrs. Sally Finora for providing the necessary assistance during the course of this research. I appreciate the help offered by Jenny Lai with XRD and SEM analysis.

I am indebted to my parents and sister in India, for unconditional support and encouragement during the course of the study. I sincerely appreciate the support provided by Mrs. Nidhi Sharma, Mr. Naresh Sharma, and Major Brijendra Singh, during my stay at the University.

Lastly, I would like to thank my friends who kept me motivated, for without them, the "extra-curricular" time spent in University and Vancouver would not have been exciting and adventurous.

Chapter 1

Introduction and Research Objectives

Phosphates are essential for all plants and animal life and are required by all the living organisms as nutrition. Plants require a total of 16 nutrients classified as macro and micro, depending upon the amount required. Phosphorous is classified as one of the nine primary nutrients (macronutrients) required by plants. A fertilizer essentially is an industrially produced material that provides the micro and the macro nutrients to the soil such that the nutrients are readily available for uptake by plants. Phosphate rock minerals are globally the primary source of phosphate for the fertilizer industry. According to a report published by FAO (2010), the global demand for phosphate fertilizer was expected to be 39.1 million tonnes in 2010 and increase annually by about 3.8% in the period 2010-2014. The global supply capacity was expected to be 40.3 million tonnes in 2010 and increase only by 3.6% in the same period.

As dictated by the fertilizer industry, the grade of phosphate ores is usually expressed as an equivalent content of P_2O_5 (phosphorus pentoxide) even though phosphorus pentoxide is not really present in the ore. As a result several minerals contribute to the P_2O_5 grade of a phosphate ore. While some of those P_2O_5 bearing minerals are considered valuable (e.g., fluorapatite $(Ca_5(PO_4)_3F)$, hydroxyapatite $(Ca_5(PO_4)_3(OH))$, francolite $(Ca_{10-a-b}Na_aMg_b(PO_4)_{6-x}(CO_3)_{0.4x}F_2))$, some are unfortunately treated as gangue because of other components of those minerals.

In the case of crandallite, the high aluminum content makes it technologically and economically unfeasible to produce water soluble phosphate by conventional methods (UNIDO and IFDC, 1998). Phosphates in fertilizers are conventionally produced by adding acid (either sulfuric acid or phosphoric acid) to ground phosphate concentrate. High aluminum content increases the acid consumption and makes the process uneconomical. To produce any type of concentrate from crandallite, it is calcined at

about 500°C. At present, Thies in Senegal and phosphate deposit of Christmas Island are the only aluminum phosphate deposits that are amenable for calcination as published in a manual by United Nations Industrial Development Organization (UNIDO) and International Fertilizer Development Center (IFDC) (UNIDO and IFDC, 1998). The product produced in Senegal is marketed by the trade name "Phospal" ("Polyphos" for animal feed use) while "Calciphos" is the product from Christmas Island (Bolland and Gilkes, 1987). Currently, the production of calciphos at Christmas island is closed. The manual also mentions that crandallite-rich Florida "leached-zone" deposits cannot be used for commercial production of calcined product as the material is low grade and variable in composition.

More than 60% of the total global marketable phosphate is produced by flotation (Abouzeid, 2008), essentially by anionic flotation of phosphate ores. The anionic flotation of these ores uses fatty acids as collectors, and certain depressants like starch and sodium silicate. The reagents used for the froth flotation of phosphate are discussed by Sis and Chander (2003), and Guimarães et al. (2005), and the references therein. As discussed in the literature review (Section 2.1), no systematic fundamental data exist on the mechanism of contamination of apatite concentrates by crandallite, whether by mechanical entrainment or true flotation.

Fatty acids are known to get selectively adsorbed on the surface and act as collectors for sparingly soluble salt-type minerals like calcite ($CaCO_3$), magnesite ($MgCO_3$), apatite etc. The chemical adsorption on the surface of these minerals renders them hydrophobic and amenable to be recovered by froth flotation. The selectivity of the process is due to a high chemical selectivity of anionic surfactants towards these minerals (Peck and Wadsworth, 1963, 1965). Although, there is no experimental data which concludes similar behaviour of crandallite with oleic acid, also a sparingly soluble salt-type mineral, the mineral is still believed to interact with oleic acid in a similar manner.

1.1   Research Objectives

Therefore, the general objective of this thesis was to characterize the surface properties of crandallite relevant to froth flotation as a function of pH and reagent concentration. The surface charge and zeta potential characteristics, along with surface wettability by water and stability of fine mineral particles towards aggregation were of primary significance. The detailed objectives can thus be summarized as follows:

1. To determine the iso-electric point of crandallite in the presence and absence of calcium ions.

2. To assess the stability of fine crandallite particles towards aggregation in the presence and absence of oleic acid and starch through turbidity measurements.

3. To demonstrate the effect of oleic acid on the wettability of crandallite under typical flotation conditions.

As a result of these fundamental studies, strategies to minimize the detrimental impact of crandallite on apatite flotation were also to be developed.

Chapter 2

Literature Review

2.1 Crandallite

Crandallite is a hydrated calcium-aluminium phosphate mineral with a chemical formula of $CaAl_3(PO_4)_2(OH)_5 \cdot H_2O$. The mineral was found by Mr. Loughlin in vein material on the dump of Brooklyn mine, in the Monzonite area of the district of Silver City, Utah (USA) (Loughlin and Schaller, 1917). The mineral was named after an engineer, Milan L. Crandall, Jr., of Knight Syndicate, Provo, Utah, USA.

Crandallite belongs to the bogummite group of the alunite supergroup of minerals (APS minerals) (Dill, 2001; Mills et al., 2009). They have a general formula $XAl_3(PO_4)_2(OH)_5 \cdot H_2O$, where X= Pb, Ba, Sr or Ca, or $CeAl_3(PO_4)_2(OH)_6$ (florencite) (Blanchard, 1972). Aluminium-phosphate minerals of the alunite supergroup do not belong to the accepted rock-forming minerals. This group contains more than 40 mineral species. Dill (2001) explains the formation of APS minerals. APS minerals occur in all types of rocks including metamorphic, sedimentary and igneous rock deposits. Both supergene and hypogene processes are responsible for the precipitation of these minerals to form complex solid solution series (s.s.s.). The chemical composition of these minerals is governed by the physico-chemical conditions during which these minerals were formed. Loughlin and Schaller (1917) studied the origins of the mineral from the associated minerals present in the dump. They concluded that crandallite may either be the latest of the primary or the earliest of the secondary minerals. Blanchard (1972) in the X-ray analysis of crandallite from Florida found that larger Sr^{++} may have substituted the smaller Ca^{++}.

The crystals of crandallite are known to occur as fibers or spherules and crusts with radial fibrous structure (Anthony et al., 2000). The crystal structure was studied in detail by Blount (1974). He suggested that crandallite consists of sheets of Al octahedra. Each of these octahedra shares the four corners with the other octahedra to form large hexagonal and

small trigonal rings. The octahedra sheets are believed to be perpendicular to the z-axis and the Ca cations lie between the sheets in large cavities surrounded asymmetrically by 12 oxygen and hydroxyl ions. Each phosphate tetrahedron shares three corners with the three Al octahedra common to a trigonal ring. The remaining unshared corner points away from the trigonal hole towards the adjacent sheet and is hydrogen bonded thereto. While analysing the structure of crandallite, Blount mentioned the existence of hydrogen bonding in the structure. This bonding occurs between the layers in a way to link together adjacent layers and every other layer. This makes the structure framework-like for crandallite.

Blanchard (1972) in his study generalized that crandallite in Florida phosphorite is a secondary mineral formed during the weathering of phosphorite (apatitic) clayey sediments. He discussed further that aluminium in the crandallite is derived from the clay minerals while P and Ca are derived from the apatite. Sr (and Ce) can only be derived from apatite and that during the weathering of apatite, Strontium (Sr) is preferentially taken up in the crandallite resulting in an enrichment of SrO.

The density of crandallite is reported in the range of 2.78-3.04 while Mohr's hardness number 5 is assigned (Anthony et al., 2000). The optical properties of crandallite are mentioned by Loughlin and Schaller (1917), who reported a refractive index of 1.605 $\pm$ .005 while working on a sample from Brooklyn mine, Utah. Greenberg and Elberty (1958) reported a refractive index of 1.620-1.630 $\pm$ .002 for a sample from Gardner Mine Ridge, Indiana. The mineral is uniaxial implying two principle refractive indices and one optical axis. The birefringence as mentioned in the literature for crandallite is weak (a value of 0.1-0.2) (Greenberg and Elberty, 1958; Loughlin and Schaller, 1917). This weak birefringence implies that there is very small, if any difference between the largest and smallest measured refractive index for crandallite.

There are certain mineral properties that should be known when a mineral is required to be separated from a group of other minerals (Salopek et al., 1992). For flotation, the sort and composition of mineral is important. It is also imperative to know the solubility of mineral in water. Most importantly, the data about the zeta potential at different pH values is indispensable when considering reagent selection and conditions for the separation of mineral.

There is very little published information about the surface properties of crandallite relevant to froth flotation. As seen from above section on crandallite, most of the data has been reported from a geologists view. Crandallite is treated as a gangue mineral in the flotation of phosphate and this may be the main reason that nothing has so far been reported which might characterize its surface. Due to the lack of literature on crandallite, it is difficult to determine the flotation behavior of crandallite based upon its naturally hydrophobicity. There is not enough data available which can discuss the effect of polymers (i.e. whether crandallite can be depressed, if it is hydrophobic) and anionic collectors (i.e. if it can be made hydrophobic). Therefore, the overall objective of this thesis is to generate some fundamental data on the zeta potential, aggregation/dispersion, and wettability characteristics of the mineral.

2.2 Stability of Mineral Suspensions

To understand the stability of suspensions, it is valuable to understand the origin of surface charges on the surfaces of mineral particles when they are dispersed in a aqueous suspension. It is also necessary to understand how these charges affect the interactions at the particle-liquid interface and interaction between other particles in a suspension. The following sections will make an effort to introduce the necessary.

2.2.1 Origin of Surface Charges on Minerals

When a particle of mineral is placed in water, its surface develops a charge. The main mechanisms that cause the development of surface charges are discussed in subsequent sections (Cosgrove, 2005; Delgado, 2002).

Ionisation of Surface Groups

Minerals which have functional groups become charged as a result of surface groups. Whenever a mineral surface has ionizable groups, e.g. hydroxyl (OH^-), such groups, depending upon the pH dissociate to form positively or negatively charged sites on the mineral surface. Such a mechanism is also referred to as surface hydrolysis, and is typical for oxide-type and oxidized minerals. This mechanism can also be induced by the polar nature of mineral surface which makes the surface capable of absorbing H^+ or OH^- from solution to form charged sites.

Similarly, minerals may acquire charge due to the presence of carbonate (CO_3^{-2}), phosphate (PO_4^{+3}) groups on their surface. Speciation upon hydrolysis of these ions is known to occur at different pH values in solution.

Preferential Adsorption of Ions from Solution

Certain ionic species may get adsorbed onto the surface of the mineral imparting an electrical potential to the mineral surface. This mechanism of charge generation is usually observed when ionic surfactants are added into the colloid and the mineral surface has high affinity for the added surfactant. Certain chemicals are used to disperse particles in a colloid and are referred to as dispersants (for e.g. the printer cartridge has dispersants). Adsorption of dispersants also modifies the surface charge of fine particles.

Preferential Dissolution of Constituent Ions in Solution

Water molecules are polar due to the presence of strong covalent O-H bonds. This nature of water allows it to form hydrogen bonds with other polar/covalent materials. This surface hydration due to hydrogen bonds by water causes all salt-type minerals to be soluble in water to some extent. This is characterized by the solubility product (K_{SP}) of the mineral. K_{SP} is the product of the solubilities of the ions in moles per liter (mol/l).

K_{SP} of crandallite can be calculated from the assayed ion concentration of Ca^{+2}, Al^{+3} and PO_4^{-2} as in equation 2.1.

$$K_{SP} = [Ca^{+2}][Al^{+3}]^3[PO_4^{-2}]^2[\text{OH}^-]^5 \qquad (2.1)$$

However, the PO_4^{-2} ion is known to occur as different hydrolysed species like $[\text{HPO}_3^-]$ and $[\text{H}_2\text{PO}_2^-]$ (Hoffmann et al., 1989) based on the pH of aqueous solution. This makes the calculation of solubility product difficult for crandallite. There is no data available in the literature which calculates or mentions the K_{SP} for crandallite.

As soon as an ion goes into solution, it leaves an oppositely charged site on the mineral surface. This solubility of salt-type minerals is reversible. Dissolution leads to the formation of surface charges on the surface of salt-type minerals. This mechanism of surface charge development is referred to as differential (or preferential) dissolution of constituent ions. When an excess of anions is present in solution, then the mineral will preferentially release cations into the solution to satisfy

the solubility product. This will cause the mineral surface to acquire a net negative charge. Similarly, the presence of excess cations will induce differential dissolution of mineral-forming anions and the mineral surface will be positively charged.

Isomorphous Substitution in Mineral Lattice

In crystal lattices of certain minerals, one atom may be substituted by another atom of similar size. This mechanism is usually observed in clays where a certain number of Si^{+4} atoms in the lattice are observed to be substituted by similarly sized Al^{+3} ions. As a result, the crystal itself has a permanent structural charge which results in the development of surface cations. These ions are easily exchanged in solution.

Adsorption and Desorption of Lattice-forming Ions

There are two kinds of ions- inert and potential-determining ions (p.d.i.). *Potential-determining ions are species which by virtue of their electron distribution between the solid and liquid phases determine the difference in Galvani potential between these phases* (IUPAC). The *Galvani potential* of a phase is the work done in taking a unit charge from infinity to a point inside the phase (Cosgrove, 2005). These are usually the ions that can easily get into the crystal sites of mineral and thus become a part of the particle surface. For crandallite, $[Ca^{+2}]$, $[Al^{+3}]$, $[PO4^{-2}]$ and [H$^+$] behave as p.d.i. and if present in the solution, are capable of affecting the surface charges of the mineral. Inert ions, on the other hand, do not affect the surface charge of the mineral.

The above mentioned mechanisms are mostly responsible for charge development. However, there might be a combination of mechanisms responsible for the origin of charges on the surface of a particle. **Preferential dissolution of constituent ions** (2.2.1) and **surface hydrolysis** (2.2.1) are the two major mechanisms that are most relevant to salt-type minerals, including crandallite. Although, generally it is believed that the preferential dissolution of constituent ions is primarily responsible for the generation of surface charges on the surfaces of salt-type minerals, infrared spectroscopic evidence shows that formation surface hydroxyl groups also plays a significant role in the surface charging phenomena (Pokrovsky et al., 2000).

2.2.2 Particle/Liquid Interactions

When a fine solid particle is placed in a solution of an electrolyte, it is acted by two forces (if the gravitational forces are ignored). It is affected by van der Waal's attraction forces and electrostatic repulsive forces. Both the attractive and the repulsive forces will be quantified in the following sections. The net force acting on the particle is determined by the balance of attractive and repulsive forces. Thus,

$$V_A + V_R = V_T \tag{2.2}$$

where V_A, V_R, and V_T are the attractive, repulsive, and net total potential respectively, experienced by the particle.

Attractive Forces

Colloidal particles can be considered to be large assemblies of atoms which have a permanent dipole. However, the motion of electrons in these atoms cause rapidly oscillating dipoles. It is energetically more favourable for the adjacent atoms to oscillate in union. This causes the fluctuating dipole to be coupled, it results in the London dispersion interactions. These interactions are non-directional and thus do not cancel out at large. These London dispersion interaction between particles leads to van der Waals forces of attraction. Hamaker (1937) calculated these attraction forces from equation 2.3, when the separation distance d between the particles is comparably smaller than the diameter of the particle D.

$$V_A = -\frac{AD}{24d} = -\frac{AR}{12d} \tag{2.3}$$

where, A is the Hamaker constant, D and R are the particles diameter and radius, respectively. The Hamaker constant (usually in the range of 10^{-20} J) is a function of the electronic polarisability and the density of the material. Hamaker constants for various materials were listed by Cosgrove (2005).

Repulsive Forces

The repulsive forces in equation 2.2 are due to the presence of electrical charges on the surfaces of particles in the liquid (water). There are various mechanisms which can contribute towards the origin of charges on the surface of a mineral and were discussed in more detail in section 2.2.

When a charged solid particle is placed in a solution of an electrolyte, an ion concentration profile develops around the particle due to the development of surface charges on its surface. Ions of the same charge sign (co-ions) will be repelled from the surface of the particle, while ions of the opposite sign (counter-ions) will be attracted towards the surface.

This ion concentration profile around a charged particle is referred to as the electrical double layer. The layer of counter-ions closest to the particle is strongly bound by the electrostatic forces and is called the "inner" or "compact" layer (also referred to as the adsorption or Stern layer). Ions further away from the surface of particle are weakly attracted to the particle surface and are loosely attached to the particle. This layer of the weakly attached ions form the "diffuse" layer (Gouy-Chapman layer).

The ion concentration profile of counter- and co-ions, expressed as the number of ions per unit volume, follows the Boltzmann distribution function. The function is defined for a particular type of ion (i) and is given by equation 2.4.

$$n_i = n_i^0 \exp(\frac{-w_i}{kT}),$$
$$w_i = ze\Psi \tag{2.4}$$

where, n_i^0 is the number of ions per unit volume in bulk solution far from the charged particle surface, k is the Boltzmann constant, and T is the temperature in Kelvin. The work done (w_i) is measured by the electrostatic energy that the ion acquires and is mentioned in equation 2.4, where z is the valency of the ion, e is the electronic charge, and Ψ is the electrostatic potential.

The net volume charge density of particles (ρ) at the interface is given by equation 2.5 (Hunter, 1993).

$$\rho = \sum_i n_i z_i e = \sum_i n_i^0 z_i e \exp(\frac{-z_i e\Psi}{kT}) \tag{2.5}$$

According to the electrostatic theory, the Poisson-Boltzmann equation gives the relation between the density of electric charge, the electrostatic potential and the distance from a flat charged surface. This is given by equation 2.6.

$$\frac{d^2\Psi}{dx^2} = -\frac{\rho}{\epsilon_w} = -\frac{1}{\epsilon_0\epsilon_r} \sum_i n_i^0 z_i e \exp(\frac{-z_i e\Psi}{kT}) \tag{2.6}$$

where x is the distance from the surface, ϵ_w, ϵ_0 are the permittivities of water and vacuum respectively, while ϵ_r is the dielectric constant (ϵ_w/ϵ_0).

The second order equation 2.6 is usually solved using the Debye-Hückel approximation. The approximation assumes that the electrical energy is small as compared to the thermal energy. Thus after the approximation the expression $ze\Psi$ is less than kT. This convenient approximation gives a simplified solution of equation 2.6 in the following form:

$$\Psi = \Psi_0 \exp(-kx) \tag{2.7}$$

where Ψ_0 is the surface potential at a distance x=0, while the constant k, is referred to as the Debye-Hückel parameter and its value is given by the equation 2.8

$$k = \sqrt{\frac{e^2 \sum n_i^0 z_i^2}{\epsilon_w kT}} \tag{2.8}$$

After putting the values of the constants into the above expression (at T=250°C), the constant k for an ion can be calculated from the equation 2.9.

$$k = 3.2881 \sqrt{\frac{\sum c_i z_i^2}{2}} \tag{2.9}$$

where, c_i is the concentration of ith ion in solution in mol/dm^3.

The term under the root sign in equation 2.9 is referred to as the ionic strength of the solution. The dimension of constant k is the reciprocal of length, thus k^{-1} is called the thickness of the electrical double layer. From equation 2.7, the thickness of the electrical double layer denotes the distance from the surface of the particle at which the electrostatic potential decreases by a factor of e (=2.71828).

It is clear from equations 2.7, 2.8 and 2.9 that the "thickness" of double layer is dependent on the concentration of electrolyte or ionic strength but independent of particle size. In dilute electrolyte solutions, the electrical double layer is extended or thick. While, at higher ionic strengths, the "thickness" of the electrical double layer decreases which is referred to as the compression of the electrical double layer. Equation 2.7 is also important as it defines the relation between electrostatic potential and the distance from a charged surface. This allows one to calculate the energy due to the repulsive forces (V_R) between the two charged particles

in a colloid.

Considering two identical spherical particles with a radius R and separated by a distance d in a colloid of dielectric constant ϵ, and assuming that the surface potential is low and constant, then the repulsive energy is the expression given by Hunter (1987) (equation 2.10).

$$V_R = 2\pi\epsilon R\Psi_0^2 \ln(1 + \exp(-kd)) \qquad (2.10)$$

According to Hunter (1987), equation 2.10 is only applicable if the electrical double layer is strongly compressed compared to the particle size i.e. when the product of kd is more than 10. If the electrical double layer is extended i.e. the product of kd is less than 5, then an approximate formula for expressing repulsive interactions can be used as originally proposed by Verwey and Overbeek (1948).

$$V_R = 2\pi\epsilon R\Psi_0^2 \exp(-kd) \qquad (2.11)$$

Total Force and the Basis of DLVO Theory

The net total potential experienced by the particle in a colloid is obtained by substituting the values of V_R (2.10 or 2.11) and V_A (2.3) in equation 2.2. These equations are the basis of the DLVO theory whose original form is given in equation 2.12. The DLVO theory of colloidal stability was proposed independently by Derjaguin and Landau (1941) and Verwey and Overbeek (1948).

$$V_T = -\frac{AR}{12d} + 2\pi\epsilon R\Psi_0^2 \ln(1 + \exp(-kd)) \qquad (2.12)$$

If the solids-liquid suspension can be considered as a concentrated colloidal system, then the rules of the DLVO theory can be applied to the suspension.

2.2.3   Colloidal Stability

In all industrial applications, solid-liquid dispersions show a wide solid particle size distribution ranging from nanometers (10^{-9}m) to several millimeters (10^{-3}m) in diameter. Solid-liquid dispersions are commonly classified as colloidal systems or suspensions. Colloids usually consist of particle sizes in the size range of 1nm to 1μm (Everett, 1988; Tadros, 1986). Suspensions generally cover particle size are coarser than the colloidal system (more than 1μm). However, for simplification, an approximation can be made such that any solid-liquid suspension can be looked at as a

concentrated colloidal system. This approximation allows the applicability of the classic rules of colloid chemistry (Araujo, 1988).

The two widely used methods to increase the stability of the colloid are electrostatic stabilization (as explained by the DLVO theory) and polymeric stabilization as discussed below.

DLVO Theory and Stability of Colloids

The discussion of the DLVO theory emphasize the importance of surface charge on the stability of colloids. In a suspension, when the attractive forces are dominant over the repulsive forces, the particles agglomerate, a process referred to as coagulation and the colloid is said to be unstable. On the other hand, if the repulsive forces are dominant, the particles in colloid stay dispersed and the colloid is termed stable.

Uncharged particles undergo rapid coagulation under the effect of attractive forces in the absence of repulsive forces. Therefore, when the surface potential of particles is zero, the turbidity of the suspension decreases drastically. This sticking together of particles due to the attraction forces and changes in the electrical double layer around particles is termed as **coagulation** (Hunter, 1993).

The DLVO theory was reformulated after non-DLVO forces were also found to affect the stability of colloids and suspensions. The hydrophobic and hydration forces also called as structural forces result from the preferential orientation of water molecules at the water-solid interface. As the terms suggest, hydrophobic forces cause the surface to repel water while the hydration forces make the surface to attract water. The term "extended" or "modified" is used when structural forces are included in the total force balance.

In the case of strongly hydrophilic solids characterized by contact angles lower than 20°, the hydration repulsive forces start to play the dominant role (Churaev, 1995). This leads to surprisingly stable dispersions, even at the point of zero charge (p.z.c.), when the system should aggregate. *A surface charge is at its point of zero charge when the surface charge density is zero. It is a value of the negative logarithm of the activity in the bulk of the charge-determining ions* (IUPAC). At p.z.c. the surface of a mineral has a net zero charge and is covered by uncharged functional groups.

A charged stabilized suspension is very sensitive to addition of salts, particularly containing ions of higher valency. When a colloid is stabilized by electrostatic repulsion, there is only a kinetic barrier to prevent agglomeration. Thus the colloid becomes unstable at high solids concentration (Cosgrove, 2005).

Polymeric Stabilization of Colloids

Colloids can also be stabilized using high molecular weight polymers. These polymers affect the interactions between the particles in colloid thus changing their stability. The key mechanisms by which this can be accomplished are (Cosgrove, 2005):

1. A polymer can be chemically adsorbed on the surface of the particles in the colloid. This attachment of polymers leads to repulsion between particles. This mechanism is referred to as **steric stabilization**.

2. Some polymers may not get adsorbed on to the surface of particle but may still induce attraction between them. This is referred as **depletion interactions**.

3. Some polymers induce aggregation by adsorbing onto two particles simultaneously, a process commonly known as **bridging flocculation**.

A detailed discussion on stabilization of colloids by polymers was discussed by Napper (1983). These are also mentioned by Cosgrove (2005) in the section on "Effect of polymers on colloidal stability". The term **flocculation** is used to describe the formation of loose aggregates of particles linked together by a high molecular weight polymer (Hunter, 1993).

2.2.4 The Zeta Potential and its Significance

The surface potential of the mineral surface (Ψ_0) can only be calculated accurately for simple salt-type minerals like barite ($BaSO_4$), calcite ($CaCO_3$) or silver halides (AgCl, AgI) provided there is no interfering ion present in equilibrium with the corresponding crystal-forming minerals as they effect the surface potential of mineral (these ions are termed as potential determining ions or PDI). Even if the surface potential of mineral surface can be calculated or measured accurately, it would hardly be of any use in predicting the behaviour of fine particles in suspension. Surfactants added into the colloid may get adsorbed onto the mineral surface and alter

the surface potential. Thus another particle approaching the surfactant coated particle will sense an effective surface potential different from the original surface potential (Ψ_0). The best estimate of this effective potential is the potential of the diffused part of the electrical double layer.

The measurement and exact calculation of the potential of the diffused part of double layer (referred to as Stern Potential) is difficult and often impossible. This is due to the fact that different polymers and ions get adsorbed on the surface of mineral to different degrees. The exact position and thickness of Stern layer is thus difficult to determine. Therefore, we can only determine the effective potential at a certain distance away from the surface, referred to as the zeta potential (denoted by the Greek letter ζ). For all practical purposes, this potential is assumed to be the potential of the Stern layer.

The fine colloidal particles move randomly in an electrolyte. As they move, the diffused layer of electrical double layer (EDL) is sheared off and the Stern layer is exposed to other approaching particles. This makes the ζ potential even more important than the surface potential for a colloid. The ζ potential (or Stern potential) can also be defined as the effective energy barrier that a charged particle senses as it approaches another charged particle. In purely physical terms, it is the work needed to bring a charge from infinity to some point where the Stern layer just ends (d). Thus the ζ potential (in Volts) can be given by equation 2.13.

$$\zeta = \frac{q}{4\pi\epsilon d} \tag{2.13}$$

where, q is the unit charge, ϵ is the permittivity of water and d is the distance from the center of the particle plus the thickness of Stern layer.

The ζ potential of a colloidal system can only be measured when the particles are forced to move within an electrolyte solution such that the Stern later is exposed. The methods of measurement of ζ potential are collectively referred to as the electrokinetic effects to reflect the fact that they involve some form of particle motion with respect to the surrounding electrolyte medium.

The ζ potential measurement can be made using four well known techniques as described by Hunter (1993). Electrophoresis techniques are widely used to measure ζ potential for flotation studies as these

measurements are simple and can be carried out quickly. The mineral needs to be finely ground for these measurements and the suspension must have low solids content.

When a constant electric field is applied to a colloidal suspension palced between two electrodes, charged colloidal particles move towards one of the electrodes depending upon the sign of the surface charge. The velocity of their motion is proportional to the surface charge. Thus any given particle in the colloid will be subjected to two forces: the electrical force and the viscous (or drag) force.

The electrical force acting on the particle is given by equation 2.14.

$$F_{el} = \sigma_0.E \tag{2.14}$$

where, σ_0 is the surface charge and E is the strength of the electrical field (applied voltage divided by the distance between the electrodes).

The particle in motion in the electrolyte also experiences a drag force given by equation 2.15. For very small spherical particles in a continuous viscous fluid the viscous force is given by the Stokes's law:

$$F_{visc} = 6\pi\eta a v \tag{2.15}$$

where η is the liquid viscosity, v is the particle velocity, and a is the particle radius assumed to be now equal to the actual radius r plus the thickness of the Stern layer.

During electrophoresis, the fine particle quickly reaches a steady migration velocity, v, when the acceleration electric force equals the retarding fictional force. Under equilibrium conditions, the two forces acting on the particle should cancel out each other i.e. $F_{el}=F_{visc}$, which after rearrangement gives us equation 2.16.

$$v = \frac{\sigma_0 E}{6\pi\eta a} \tag{2.16}$$

The ζ potential for this particle was already defined in equation 2.13. After substituting the value of σ_0 from that equation to equation 2.16, the velocity of the particle (v) is related to ζ potential as given in equation 2.17.

$$v = \frac{2\epsilon\zeta E}{3\eta} \tag{2.17}$$

Equation 2.17 is usually expressed in terms of the electrophoretic mobility (ν_E), which is an intrinsic property of the particle (equation 2.18). Equation 2.18 is often called the Hückel equation (1924).

$$\nu_E = \frac{2\epsilon\zeta}{3\eta} \qquad (2.18)$$

Henry (1931) introduced a correction function *f(ka)* to the Hückel equation to account for the effect of particle size. With the correction function included, the Hückel equation becomes the Henry equation 2.19.

$$\nu_E = \frac{2\epsilon\zeta}{3\eta} \cdot f(ka) \qquad (2.19)$$

The correction function *f(ka)* varies smoothly from 1 to 1.5 as *ka* changes from 0 to infinity. Practically, *f(ka)* can be taken as 1 when *(ka)* $\leq$ 0.5. When *(ka)* is small, the charged particle can be treated as a point charge and the Henry equation becomes the Hückel equation. It is generally only valid for studies of particles that are suspended in a non-aqueous media of low conductance (Cosgrove, 2005).

At the other extreme, when $ka \geq 300$, *f(ka)* approaches a value of 1.5 and the Henry equation becomes the Smoluchowski's equation (2.20) (Delgado, 2002; Hunter, 1993). When *(ka)* is large, the particle-electrolyte surface can be treated as a flat sheet (Cosgrove, 2005).

$$\nu_E = \frac{\epsilon}{\eta}\zeta \qquad (2.20)$$

Another way to state the applicability of the two equations is in terms of the thickness of the EDL. The Smoluchowski equation is applicable only to systems in which the EDL is thin compared to the particle size. At the other extreme, when the EDL is thick compared to the particle size, the Hückel equation applies. It is important to find the value of *ka* for the colloid system, to correctly identify the equation to be used while measuring the ζ potential from the electrophoretic mobility.

For the crandallite suspensions tested in this thesis, for which the zeta potential was measured using electrophoretic mobility, the *ka* can be calculated as follows. The average particle size (d_{50}) of the sample of crandallite was 3.0μm (in appendix Figure B.3). 0.01N NaCl was used as the electrolyte for all the experiments. From equation 2.8, putting the

values of all the constants at a room temperature of 25°C, the ionic strength is found to be 0.01 mol/dm^3, which gives a k value of $0.32881 nm^{-1}$. Finally, the value of *(ka)* is 990.

Thus a very important conclusion can be drawn that can be used for the calculation of the zeta potential from electrophoretic mobility data. It is evident from the value of ka for crandallite suspension ($ka_{crandallite}$=990) that the Smoluchowski's equation is valid to obtain the ζ potential. It is also clear from this discussion that the thickness of EDL $(1/k)$ is about 3.0nm.

The iso-electric point (i.e.p.) of a mineral is the pH value at which its ζ potential is zero. The iso-electric point (i.e.p.) and point of zero charge (p.z.c.) are often used interchangeably. The i.e.p of a mineral is same as its p.z.c. only if there is no specific adsorption of ions. In this condition, the inner layer charge density is also zero and the surface charge is balanced by the ions in the diffuse part of the double layer (Hunter, 1993).

Significance of Zeta Potential

The electrical double layer and subsequently the zeta potential are important in many mineral processing operations, particularly in froth flotation (Fuerstenau and Pradip, 2005; Salopek et al., 1992). Some of these are mentioned below:

1. Electrical double layer controls the flocculation and dispersion behaviour of mineral suspensions.

2. The sign and magnitude of the zeta potential controls the adsorption of flotation reagents.

3. A highly charged surface may inhibit the adsorption of chemically adsorbing reagents.

4. Electrical double layer interaction controls the formation of slime coatings.

5. Surface charges dictate the fine particle/air bubble/oil droplet interactions.

The ζ potential can help in the choice of appropriate flocculants but a definitive valuation can only be given after sedimentation studies (Salopek et al., 1992).

Chapter 3

Experimental Procedures

3.1 Materials

3.1.1 Minerals

The minerals, apatite and crandallite, used in the experiments were first characterized by various techniques that will be discussed in section 3.2.

Crandallite

Variscite rock samples containing crandallite were obtained from the Clay Canyon deposit near Fairfield, Utah, USA. The rocks (approximately 2 by 2 inches) contained only a few bands of the mineral of interest and needed to be separated from various other associated minerals which included but not limited to variscite, carbonate-fluorapatite, alunite, calcite and quartz. Figure 3.1 shows the different rocks that were obtained and were used to prepare a high purity sample of crandallite.

As crandallite was associated with so many mineral species, the separation required careful handpicking using hammer and chisel. Figure 3.2a shows the crandallite sample after hand picking. It was a very difficult and time consuming process to delicately take only crandallite out by just using the visual indications (color and texture) to locate the mineral in the host rocks. It is very difficult even for geologists in field to distinguish one mineral from another of alunite supergroup (APS minerals) by using a hand lens and a hammer. This is because the outward appearance of these minerals is often not very distinctive (Dill, 2001). So extreme care was required while liberating selectively only the crandallite minerals from the rock.

The handpicked sample was pulverized in a ceramic mill to minimise contamination with iron to obtain a d_{50} of 62μm (as "ceramic mill" in Table 3.3. The Rosin-Rammler plot is shown in Appendix in Figure B.1. Figure 3.2b shows the material obtained after milling in ceramic mill. This

(a)

(b)

(c)

Figure 3.1: Rocks containing crandallite and gangue minerals as obtained from Clay Canyon deposit near Fairfield, Utah, USA. The arrows in different sub-figures indicate crandallite.

(a) Crandallite sample after handpicking from the rock samples.

(b) Crandallite sample after being milled in a ceramic mill.

Figure 3.2: Sample preparation of crandallite.

step was the first step towards preparing the sample for the entire test program.

This sample was dry pulverized in stages in a SPEX mill using alumina media (balls) to obtain a final d_{50} of 3μm. The first milling for two minutes produced a sample with a size distribution mentioned in Table 3.3 as "SPEX Mill 1". The Rosin-Rammler plot is shown in Appendix in Figure B.2. The sample was again pulverized in the SPEX mill for another five minutes to obtain the final size distribution. The Rosin-Rammler plot obtained from Malvern Mastersizer predicted a maximum particle size of about 40μm in the final sample as shown in Appendix in Figure B.3 and Table 3.3 as "SPEX Mill 2".

The selection of the final particle size distribution was driven by the industrial practice at the Agrium-Kapuskasing Phosphate Operations (Kapuskasing, Ontario). The feed to phosphate flotation is deslimed using cyclones at about 20-25 microns (Nanthakumar et al., 2009). Crandallite is reported to accumulate in the slimes fraction in typical apatite flotation feeds. This particle size distribution of crandallite was also fine enough for the electrophoretic measurements. Also, any subsequent size reduction using SPEX mill could cause excessive contamination of the sample by iron. A total of only 13g finely powdered sample was finally obtained and used for the entire experimental program. Figure 3.3 represents the procedure adopted for sample preparation and analysis of the fundamental surface properties of crandallite.

Mineral identification of APS minerals normally requires sophisticated analytical techniques which include Atterberg settling methods, XRD, TEM-EDX, SEM, XRF etc., (Dill, 2001). To identify crandallite in the sample, a powder X-ray diffractometer (XRD) was used. The results of the XRD are shown in Table 3.1. The Rietveld refinement plot for a representative sample of apatite is shown in Appendix in Figure A.1. The SEM picture of the sample showed very little contamination by other interfering species such as iron, copper, silica etc.

Pictures of crandallite were taken under a SEM. Figure 3.4 shows the shape and texture of the crandallite particles at various magnifications. Energy Dispersive X-ray Spectroscopy (EDX) data obtained from SEM was also used to confirm the presence of crandallite in the sample. EDX plots are shown in Appendix in Figures C.4 and C.5 for a sample of crandallite.
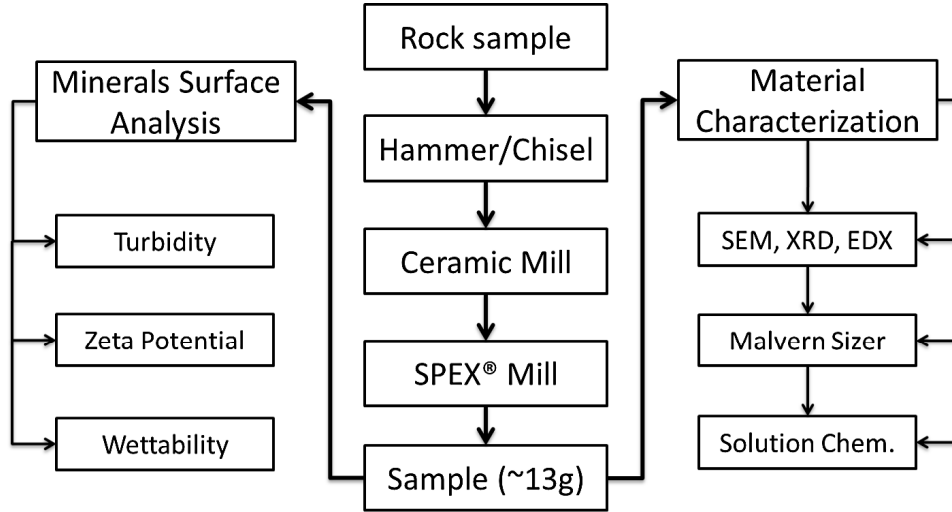
Figure 3.3: Block diagram representing the procedure for sample preparation and analysis.

Table 3.1: Results of quantitative phase analysis for crandallite sample (XRD Rietveld).

Mineral	Ideal Formula	Wt.%
Crandallite	$CaAl_3(PO_4)_2(OH)_5 \cdot H_2O$	91.0
Quartz	SiO_2	2.4
Plagioclase	$NaAlSi_3O_8 - CaAl_2Si_2O_8$	5.2
K-Feldspar	$KAlSi_3O_8$	0.4
Apatite	$Ca_5(PO_4)_3(FClOH)$	0.6
Variscite	$AlPO_4 \cdot 2\,H_2O$	0.4
Total	-	100

Apatite

Fine apatite was prepared from a clean -38μm sample obtained from Agrium-Kapuskasing Phosphate Operations (KPO). This sample was dry milled in a SPEX mill for 3 minutes with a mix of alumina and zirconia balls. The quantitative XRD analysis of the sample is shown in Table 3.2 indicated that most of the apatite was in the form of fluorapatite (82%) while the rest was present as hydroxylapatite (13%) and both minerals are fully recoverable by froth flotation at KPO. The analysis indicated the presence of small amounts of pyrite and quartz. This apatite sample was used for wettability tests in the presence of oleic acid to compare the response of crandallite to the well known response of apatite.

A particle size analysis of the sample was performed by Malvern Mastersizer. A d_{50} of about 1.8μm and a maximum particle size of about 17μm is observed for the sample. The Rosin-Rammler plot of the analysis is shown in Appendix in Figure B.4.

Figure 3.4 shows the shape and texture of the apatite particles at various magnifications. EDX plots for a sample of apatite are shown in Appendix in Figures C.6 and C.7. The EDX plot in Appendix in Figure C.6 confirms that the mineral in the sample is apatite, however Figure C.7 shows that the sample might be contaminated with pyrite. This contamination is also confirmed from the XRD results as shown in Table 3.2. The Rietveld refinement plot for a representative sample of apatite is shown in Appendix in Figure A.2.

Table 3.2: Results of quantitative phase analysis for clean apatite sample (-38μm) (XRD Rietveld).

Mineral	Ideal Formula	Wt.%
Fluorapatite	$Ca_5(PO_4)_3F$	82.3
Hydroxylapatite	$Ca_5(PO_4)_3(OH)$	13.4
Pyrite	FeS_2	3.0
Quartz	SiO_2	1.1
Zircon	$ZrSiO_4$	0.2
Total	-	100

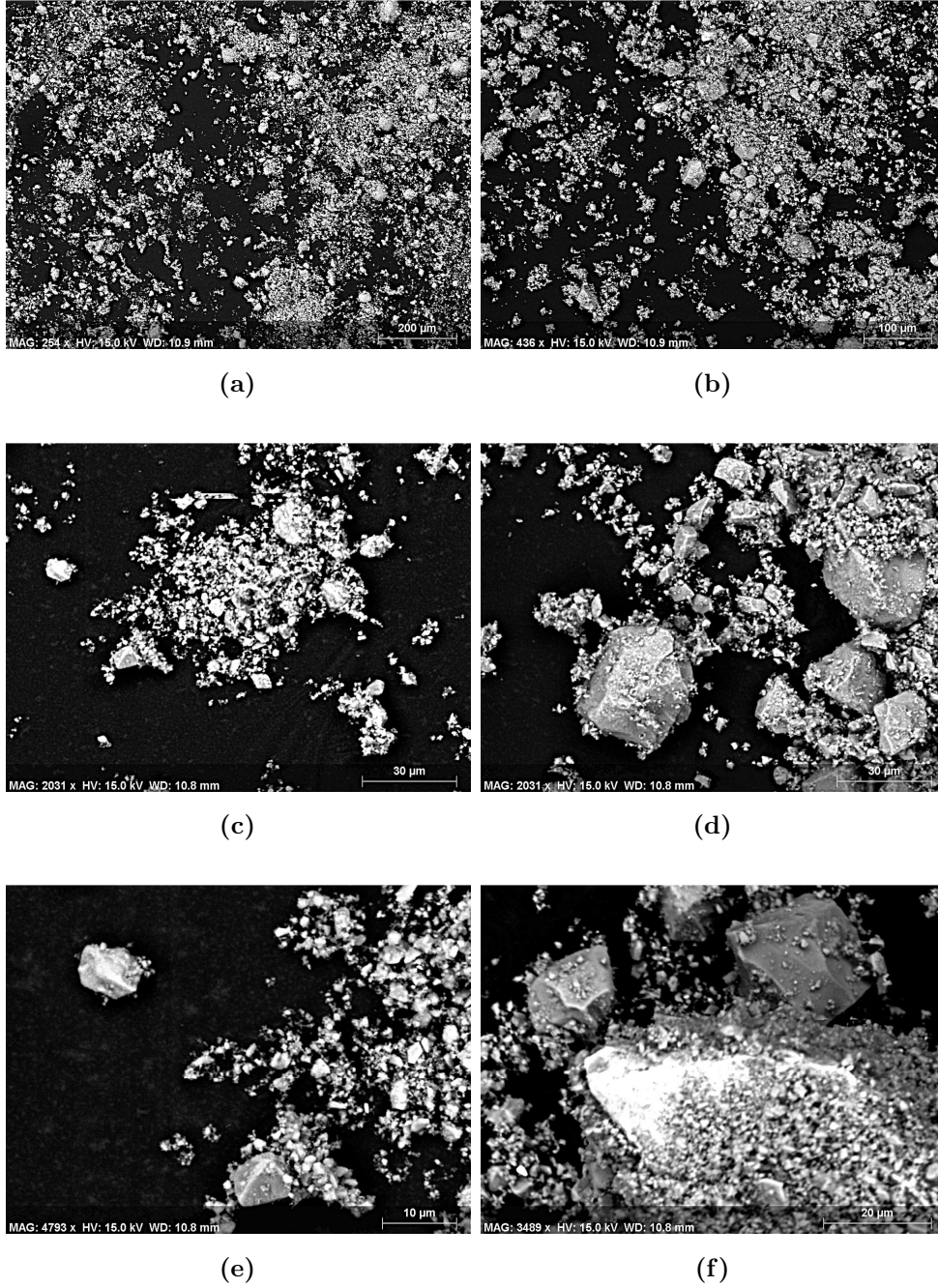**(a)**

(b)

(c)

(d)

(e)

(f)

Figure 3.4: SEM picures of crandallite (Figure 3.4a, Figure 3.4c & Figure 3.4e) and apatite (Figure 3.4b, Figure 3.4d & Figure 3.4f) at different magnifications.

It is clear from the Figure 3.4 that both crandallite and apatite have same type of grain structure. It is so similar that it is nearly impossible to distinguish one from another by just looking at the grains under a microscope. Both minerals exhibit the presence of competent crystals of various sizes. The grain size of crandallite appears to be smaller than that of apatite (at similar magnification levels). Also, the grain boundaries do not appear to be sharp. The blunt edges may have been caused due to abrasion during the pulverizing stage of sample preparation.

3.1.2 Reagents

Hydrochloric acid (HCl) and sodium hydroxide (NaOH) solutions were used for adjusting the pH of the solution during experiments. De-ionized water was used during all the experiments and to prepare the reagents.10_{-2}N sodium chloride (NaCl) solution was used as the background electrolyte for all the experiments. Fresh starch and oleic acid solutions were prepared for a daily batch of experiments.

Corn starch was provided by Casco Industrial. As starch is insoluble in water, a solubilization procedure known as gelatinization was used to make it soluble (Guimarães et al., 2005). A 3% stock starch solution was prepared by first dissolving 0.30g NaOH pellets in 3g water. 0.90g of starch was then added to 25.80g of water and agitated. NaOH solution prepared before was then added to the starch solution and the mixture was agitated for 30 minutes. This starch solution was diluted with de-ionized water as required.

Oleic acid of purity >99% was obtained from Sigma Aldrich. Oleic acid was saponified using NaOH pellets. A stock oleic acid solution was prepared by adding NaOH in a stoichiometric ratio of 1:1. The solution was then agitated for 30 minutes. A fresh stock solution was prepared and used only for 6 hours as oleic acid and its derivatives slowly decompose under the influence of air and light (Mularczyk and Drzymala, 1996).

3.2 Equipment and Methods

3.2.1 Equipment

Sample preparation was done using a hammer and chisel. A Brinkmann Retsch ceramic mill/pulverizer and SPEX8000M mixer/mill were used to

pulverize the crandallite sample. Autosorb®-1 was used in the study to measure the surface area of crandallite and apatite samples. The particle size distribution for both crandallite and apatite was obtained using Malvern Mastersizer 2000.

A Philips XL30 electron microscope with Bruker Quanta 200 energy-dispersion X-ray microanalysis system with Xflash 4010 SDD detector was used for digital imaging of crandallite and apatite. McCrone Micronising Mill was used to pulverise the crandallite sample before being analyzed by X-ray powder diffractometer. Bruker D8 Focus Bragg-Brentano diffractometer was used to collect X-ray powder-diffraction data.

Hach-2100AN turbidimeter was used to measure the turbidity values of crandallite suspensions. The electrokinetic measurements were performed using a ZetaView® PMX 100 electrophoretic instrument (Particle-Metrix GmbH, Diessen, Germany). Goniometer was used to measure the contact angle of the fine sample on a filter paper. A FTA1000 B class drop shape instrument (provided by First Ten Angstroms) was used to produce water drops of desired size. A 1-6010 Navitar microscope optical system was attached to the assembly. FTA32 software provided by First Ten Angstroms was used to analyse the pictures for contact angle values from the images obtained from the optical system.

A Fisher Scientific accumet Excel XL50 meter was used to measure the pH of the suspensions. A Fisher Scientific FS30 Ultrasonic Cleaner was used to disperse the particles in the solution. A Sorvall Biofuge Primo centrifuge was used during the analysis of solution chemistry of crandallite. IKA ®-KS 4000 ic control was used to condition the suspension for turbidity measurements. A hot plate with magnetic stir was used to condition the solids before zeta potential and contact angle measurements. Crandallite and apatite particles were filtered on 0.1μ millipore filter paper. A Welch standard lab duty oil-free pump (Model no. 2522B-01) was used to apply vacuum during filtration. All measurements and dilutions were made on mass basis using a Denver PI-225D (220g x 0.01mg) balance.

3.2.2 Methods

Powder X-ray Diffractometry

The sample was reduced to the optimum grain-size range for quantitative X-ray analysis (<10 μm) by grinding under ethanol in a vibratory McCrone Micronising Mill with agate pellets for 5 minutes. The X-ray diffractogram was analyzed using the International Centre for Diffraction Database PDF-4 and Search-Match software by Siemens (Bruker). Step-scan X-ray powder-diffraction data were collected over a range 3-80°2θ with CoKa radiation. The long fine-focus Co X-ray tube was operated at 35 kV and 40 mA, using a take-off angle of 6°. X-ray powder-diffraction data of the sample were refined with Rietveld program Topas 4.2 (Bruker AXS). The quantitative amounts reported are the representative amounts of crystalline phases normalized to 100%.

Scanning Electron Microscope and Energy Dispersive X-ray Spectroscopy

The pulverized (SPEX milled) samples of crandallite and apatite were attached to a conductive carbon adhesive. This was stuck to aluminum stubs and the carbon coated to create more conductivity. The stubs were then loaded into the vacuum chamber of the scanning electron microscope (SEM). The images were taken in the backscatter electron mode (BSE) at different magnifications. The beam was at 15kV and spot size was 6. Energy-dispersive X-ray spectroscopy (EDS/EDX) data were collected for the same samples.

Particle Size Analysis

Malvern Mastersizer 2000 was set to process the particle size ranging from 0.020 to 2000 μm. The refractive index was set to 1.618 (Greenberg and Elberty, 1958), while a low absorption of 0.1 was set for analysis. A general purpose analysis model was employed for studying the particle of the samples. The sample containing tank was stirred at 2000 rpm to effectively disperse the particles in water.

The size analysis procedure was slightly modified from as performed by Abidin et al. (2009) based on the sample characteristics. A small amount of prepared sample was added to the stirred tank containing water, where they were introduced into the dispersion module, until an adequate

Table 3.3: Malvern size analysis of crandallite after each milling stage.

Sample	d_{10P}	d_{50P}	d_{90P}
Milling Type	(μm)	(μm)	(μm)
Stage 1: Ceramic Mill	1.40	62.76	344.41
Stage 2: SPEX Mill 1	0.82	5.10	36.96
Stage 3: SPEX Mill 2	0.70	3.04	14.30

obscuration level was obtained and the laser obscuration was stable ($\pm$ 0.2%). The ideal obscuration level ranged from 10.0 to 20.0. Specimens were dispersed in water in the stirred tank of Mastersizer by ultrasonication for 10 minutes before measurement. This was necessary as particles were agglomerated. A total of two measurement cycles were carried out for each sample and the average value was taken recorded. This was repeated for three samples and an average of the three results was reported. The samples particles' specific surface area, surface weighted and volume weighted mean diameters were determined along with the d_{10}-, d_{50}- and d_{90}-cumulative undersize.

BET Analysis

BET analysis (named after S. Brunauer, P.H. Emmet and E. Teller) was performed on the samples of crandallite and apatite to determine the surface area of the mineral. BET analysis was performed on the sample of crandallite and apatite using a 6mm small bulb cell with glass tube placed inside. The outgassing was carried out using helium gas (He) at room temperature (25°C). This outgassed sample was tested after 23 hours by checking the outgass pressure rise limit (set at 50 microns/minute or 0.05 mmHg/minute). Once the sample passed the outgass test, it was removed from the outgass station and transferred to the sample position. Eleven point BET analysis was performed on the outgassed sample using nitrogen gas (N) as the adsorbate.

Solubility Analysis of Crandallite

The crandallite sample obtained after pulverizing was analyzed to study the solubility of the mineral at different pH values. A small amount (0.01g) of crandallite was conditioned with 100g of electrolyte solution (0.01N NaCl).

The solution was kept in an ultrasonic bath for 4 minutes to disperse the solids. A total of three such solutions were prepared and conditioned for 35 minutes at pH values of 6.3 (natural), 7.0 and 9.8. Lower pH values were not tested in order to avoid excessive dissolution of the mineral under acidic conditions. The pH after conditioning was recorded and the solution was centrifuged for an hour at a relative centrifugal force (RCF) of 10,000 g using a Sorvall Biofuge Primo centrifuge. After centrifuging, the solution was decanted into sample bottles and submitted for elemental analysis by inductively coupled plasma (ICP).

Turbidity Measurements

Calibration of Hach-2100AN turbidimeter was done using six Formazin turbidity standards with turbidity values from <0.1 to 7500 NTU (nephelometric turbidity units). Turbidity measurements were carried out at room temperature (24°C).

0.035g of crandallite sample was weighed and added to 25.0g of electrolyte solution (0.01N NaCl) in a clean standard 35mL vial. The solids in the solution were then dispersed in an ultrasonic bath for a minute. A known amount of starch or oleic acid was added and pH was adjusted as desired. The vial was then put into a shaker for a period of 15 minutes and the pH was adjusted during this period if necessary. After a further conditioning period of 30 minutes the final pH was recorded and the vial was put into the chamber of the turbidimeter. The turbidity value was then recorded every five minutes for a period of 45 minutes. At least three experiments were conducted for reproducibility under a given set of experimental conditions. A mean turbidity value with standard error was calculated at a given pH value.

Zeta Potential Measurements

The electrokinetic measurements were performed using a ZetaView® PMX 100 electrophoretic instrument (Particle-Metrix GmbH, Diessen, Germany) at room temperature (24°C). The instrument is capable of measuring an entire distribution of zeta potential values for a large population of tracked particles rather than a single average value. The sample cell was cleaned by flushing it with de-ionized water in between readings. Automatic measurement process was used for obtaining zeta potential values from the Smoluchowski equation. A typical report obtained after the analysis is

shown in Appendix in Figure E.1.

In a typical test, 100g of electrolyte (0.01N NaCl) was added to 0.01g of fine crandallite sample in a 200ml beaker. Either starch or oleic acid was added at desired concentration into the beaker as per the required experimental condition. The pH of the solution was adjusted and the solution was agitated using a magnetic stirrer for 35 minutes to reach a constant pH value.

After conditioning, the dispersion was transferred into the measuring cell using a 25ml glass syringe. Three readings of the zeta potential were obtained using different samples from the beaker. Two of such experiments were conducted for those particular conditions for reproducibility of the data. A mean zeta potential value with standard deviation were calculated at a given pH value. Zeta potential values were expressed in millivolts (mV).

Wettablility Study

Wettability techniques for fine particles are mentioned in the literature (Chander et al., 2007; Siwek et al., 1981). A few of these techniques were tested unsuccessfully including bubble pick up tests, vacuum flotation and modified Hallimond tube. All the methods to evaluate the flotability were first tried on the apatite sample mentioned in section 3.1.1 due to the very limited amount of crandallite.

It should be mentioned that the employed technique is not standard or routine (it is further discussed in section 4.5). However, considering the unsuccessful attempts to quantify the wettability of the fine minerals using other techniques, and because of the very small amount of crandallite available for testing, it was decided to test this approach using apatite and then adapt it for crandallite. Therefore, the method was first tested using apatite (whose response to oleic acid is very well known). Once this technique was validated for apatite, the results obtained were compared with the results obtained for crandallite.

0.2g sample of the mineral was first conditioned in 50ml of de-ionized water with required amount of saponified oleic acid at pH 10.5 for 30 minutes. The conditioned solids were then filtered using millipore filtering setup (Figure 3.5) using 0.10μm filter paper. The filter paper was
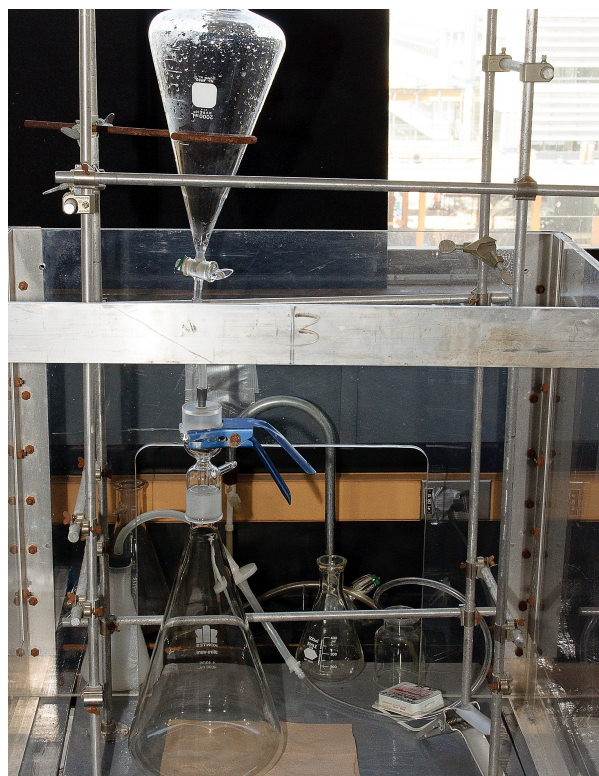
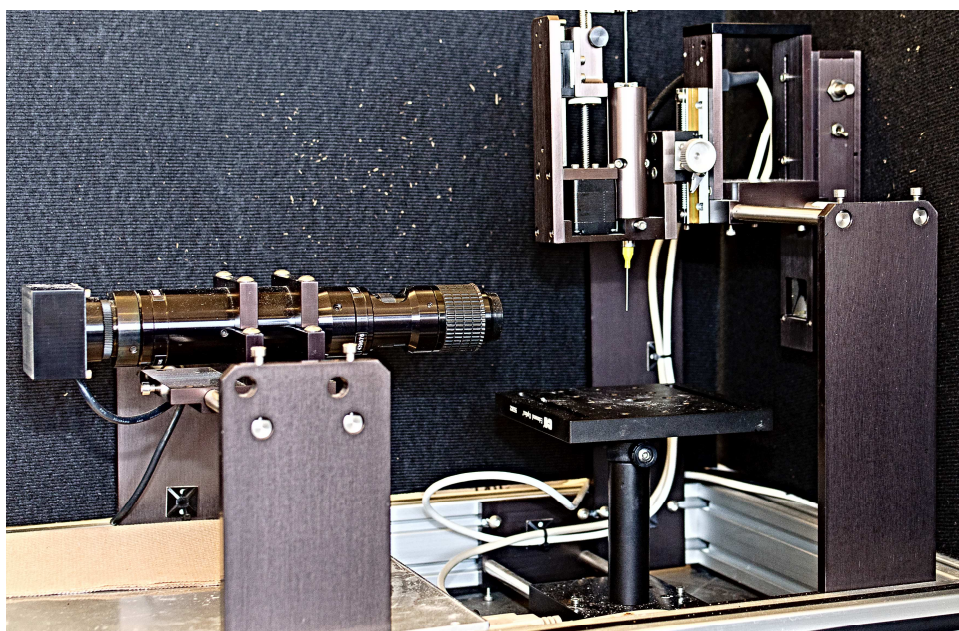**Figure 3.5:** Millipore vacuum filtration unit.

Figure 3.6: FTA1000 Class B instrument assembly used to measure contact angle.
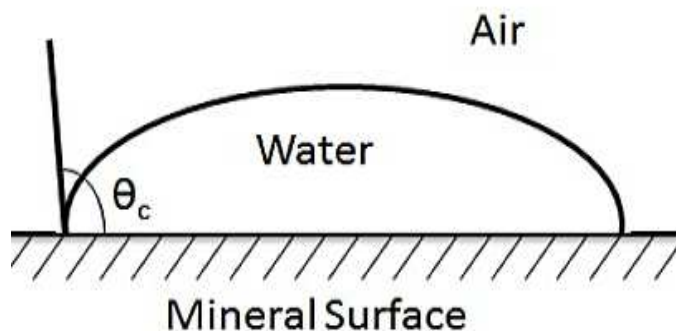
Figure 3.7: Contact angle at a solid surface as measured through the liquid phase. The mineral surface for this case was rough and not smooth.

pre-washed by filtering 500ml de-ionized water through it. About 50ml water was used as wash water to remove excess oleic acid from the surface of solids such that only adsorbed collector remained. The solids obtained after filtering were dried on a hot plate for about ten minutes which was sufficient to produce a dry surface on the filter paper. The drying process caused the filter paper to develop folds and get wrinkled. Measurement of contact angles required a smooth surface and thus the filter paper was cut into smaller sections which were planar. This cut filter paper sections were kept on glass slides and used for sessile drop measurements of contact angle.

Contact angle was measured using sessile drop method and the contact angle was measured using a goniometer. This assembly is as shown in Figure 3.6. A small water drop of volume of $5.5\mu l$ was introduced on the surface of cut sections of filter paper for contact. A snap shot was taken through the optical arrangement after within five seconds. This picture of the drop on the surface was analysed by FTA32 software to obtain the value of contact angle. A spherical fit was applied to the shape of the drop during the analysis of the pictures. The contact angle as shown in Figure 3.7 was observed. A number of readings were taken on different sections of the filter paper. This experiment was repeated for reproducibility of results.

Chapter 4

Results and Discussion

4.1 The Iso-electric Point and Baseline Stability

The solubility data for crandallite in 0.01N NaCl solution are presented in Table 4.1. It is observed that as the pH rises from the natural pH of 6.3 to 9.8, the solubility of crandallite increases in the electrolyte. It is interesting to note the magnitude of solubility. Crandallite is about four times more soluble at pH 9.75 than it is at pH 7.00. The solubility is more or less similar at pH 6.31 and 7.00.

Beck's theory on solubility (Beck, 1954) suggests that the isoelectric point (i.e.p.) will correspond to the pH of minimum solubility when the solution is in equilibrium with the solid phase. Thus solubility is an indication of point of zero charge as there is very close relation between the two. By applying Beck's theory, it is concluded that the i.e.p. for crandallite can be expected to be at pH 6.3 or lower under equilibrium conditions.

Another indication of point of zero charge (p.z.c.) is the stability of pH readings with time (Somasundaran, 1968). It was also observed during the measurements that at pH 6.3, there was no significant change in pH

Table 4.1: Solubility analysis- metals/elements in solution.

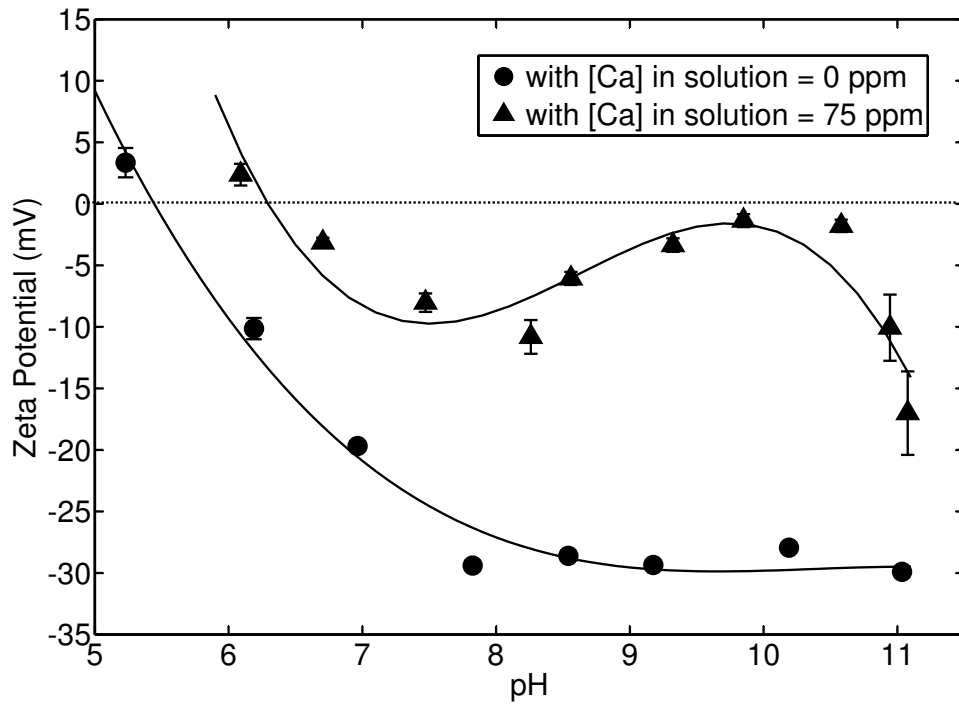| Sample	A	B	C
pH of solution	6.3	7.0	9.8
Metal/Elements	(mg/l)	(mg/l)	(mg/l)
Aluminium	0.21	0.20	1.73
Strontium	0.040	0.038	0.148
Calcium	0.59	0.52	1.29
Phosphorous	0.30	0.32	1.50

Figure 4.1: Zeta potential of crandallite as a function of pH, when conditioned with & without calcium chloride in presence of air.
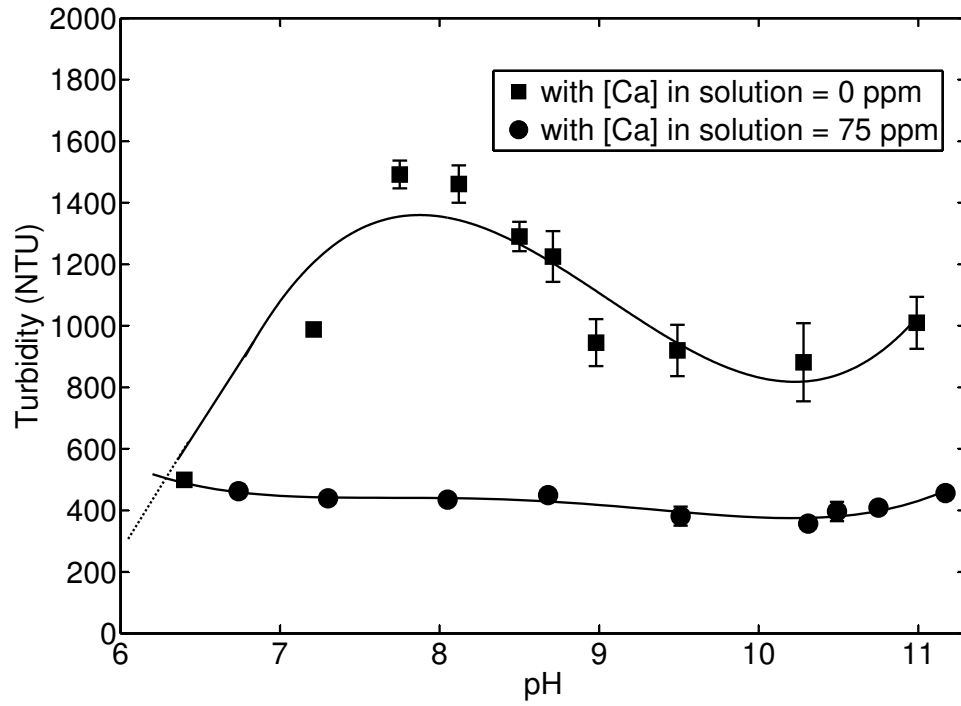
Figure 4.2: Turbidity of crandallite as a function of pH, when condition with & without calcium chloride in presence of air (1000 g/t of starch is equivalent of 1.4 mg/L).

with time. At this pH under equilibrium, equal amounts of hydroxyl and hydrogen ions are consumed by crandallite during the reactions with water. An equal number of positive and negative potential determining ions will be present; no net charge will be developed on the surface of the mineral. Thus from this, the point of zero charge can again be identified at pH 6.3 or less.

The zeta potential of crandallite in 0.01N NaCl solution as a function of pH is shown in Figure 4.1. It is noted that the i.e.p. for crandallite under equilibrium is at a pH value of 5.5. These results correlate with the earlier observations based on the solubility of the mineral and the stability of pH readings. The surface of crandallite is negatively charged at a pH greater than 5.5 but positively charged at pH lower than 5.5. The zeta potential becomes most negative at pH 8 and does not decrease substantially at higher pH.

Stable suspensions produce compact sediments which are difficult to re-disperse. High zeta potentials (either negative or positive) give rise to strong electrostatic repulsions between the particles which translates to small sedimentation volumes or higher settling times. The reverse is true for lower zeta potentials. Using turbidity as a measure of dispersion or aggregation of the crandallite particles, a good correlation can be observed with the zeta potential results.

Figure 4.2 shows the relation between turbidity measured after 45 minutes of settling and the pH of the solution. Turbidity reaches a maximum at a pH value around 8.0 which is the point of the highest zeta potential for crandallite in the tested pH range. Under these conditions the crandallite particles are most dispersed by electrostatic repulsion and settle very slowly. Slow settling results in a high turbidity value of the tested suspension. However, the turbidity of fine crandallite dispersions tends to decrease to zero at around pH 6.0, which is very close to the measured isoelectric point. At the i.e.p., the aggregation of crandallite is most advanced and the interparticle aggregates settle faster producing supernatant with the clarity of tap water.

4.2 Effect of Calcium Ions in Solution

The effect of calcium ion on the stability of crandallite is shown in Figure 4.1 and Figure 4.2. Figure 4.1 shows the impact of calcium ion at a concentration of 75ppm on the zeta potential, while Figure 4.2 depicts the effect of calcium ions on turbidity.

It can be seen from Figure 4.1 that in the presence of calcium ions, the isoelectric point of crandallite is increased slightly from about 5.5 to 6.5. However, in the pH range tested, the zeta potential of crandallite approaches a second isoelectric point at pH 10.0-10.5, where the particles are only slightly negatively charged. The zeta potential again increases after pH 10.5. Overall, the magnitude of the zeta potential of crandallite decreases across the entire pH range in the presence of a small amount of calcium, and this type of zeta potential curve is very characteristic for polyvalent metal cations. The results demonstrate a high affinity of calcium ions towards crandallite.

As a mineral-forming ion for crandallite, calcium acts not only as a potential-determining ion but also as a specifically adsorbing ion, especially at high pH when increasing amounts of $Ca(OH)^{+}$ complexes start forming in solution. The potential-determining effect of calcium in the zeta potential of the minerals can be seen in the shift of the i.e.p. from 5.5 to 6.5, while the specific adsorption at higher pH results in the gradual appearance of the second i.e.p. at pH 10-10.5. The S-shape of the zeta potential curve at higher pH is very characteristic of the specific adsorption of polyvalent hydrolyzable cations (James and Healy, 1972).

Figure 4.2 shows the corresponding changes in turbidity values of the solution after 45 minutes of settling. From Figure 4.2, it is observed that the turbidity values of crandallite are more or less constant over the entire tested pH range. Calcium ions are p.d.i for crandallite and are adsorbed on its surface which results in lowering of the electrostatic repulsion as seen from lowering of ζ potential values over the entire pH range. This results in coagulation of particles due to dominant van der Waals attraction forces which tends to lower the stability (and turbidity) of the suspension.

40

4.3   Effect of Starch

The depressing action of starch and of polysaccharides in froth flotation can be two-fold. In the case of the depression of naturally-hydrophobic minerals, the adsorption of starch renders the mineral surface hydrophilic due to the large number of hydroxyl groups on the polymer chain. However, in the case of the depression of iron and slime minerals during phosphate flotation, the role of starch is to adsorb on those fine particles and prevent the adsorption of the collector on the particle surfaces. Because starch is of high molecular weight, the polymer may also function as a flocculant, and this action of starch is often utilized in the cationic reverse flotation of quartz from flocculated hematite (Cooper et al., 1985).

Starch acts as a depressant for carbonates and ferriferous gangue minerals in phosphate ore flotation (Araujo (1988); Guimarães et al. (2005); Sis and Chander (2003)). Industrial products commercialized as corn starch usually contain starch fraction (amylopectin and amylose), proteins, oil, fibers, mineral matter and moisture. Amylose and amylopectin are the active matter of the polymer and are primarily responsible for the depressant action of corn starch (Guimarães et al., 2005). Araujo (1988) observed that various kinds of starch depress fluorapatite using sodium oleate in micro-flotation tests. Araujo observed that the depression of fluorapatite is pH-dependent and the depression action of starch at pH 7.5 is weaker than at pH 10.5. However, it was also noticed that starch does not suppress the adsorption of the collector on the fluorapatite surface. As explained further by Araujo (1988), the suppression is likely due to "the ability of adsorbed polymer molecules to interact with the adsorbing surfactant species in such a manner that the hydrophobic hydrocarbon chains are occluded within the polymer molecules."

Figure 4.3 shows the effect of starch on the zeta potential of crandallite at different pH values. In general, a similar trend was observed for all the three pH values at which the zeta potential was measured. At all the concentrations, starch does not have a very profound effect on the zeta potential of crandallite. A small decrease in the magnitude of the zeta potential can be seen at high starch dosages and these results are consistent with the non-ionic character of the polymer. Therefore, starch is not capable of changing the surface charge of the mineral, but it can only lower the magnitude of the zeta potential by moving the shear plane farther away from the mineral surface. Flocculation studies of corn starch were
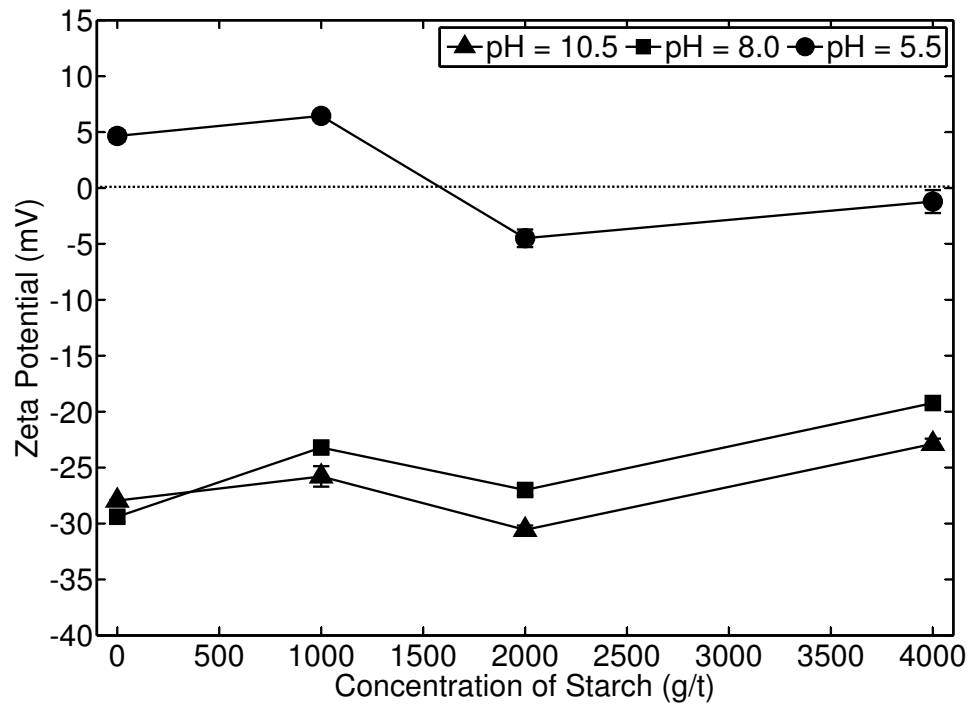
Figure 4.3: Zeta potential of crandallite as a function of concentration of starch (1000 g/t of starch is equivalent to 0.1 mg/l) at pH 10.5, 8.0 and 5.5.
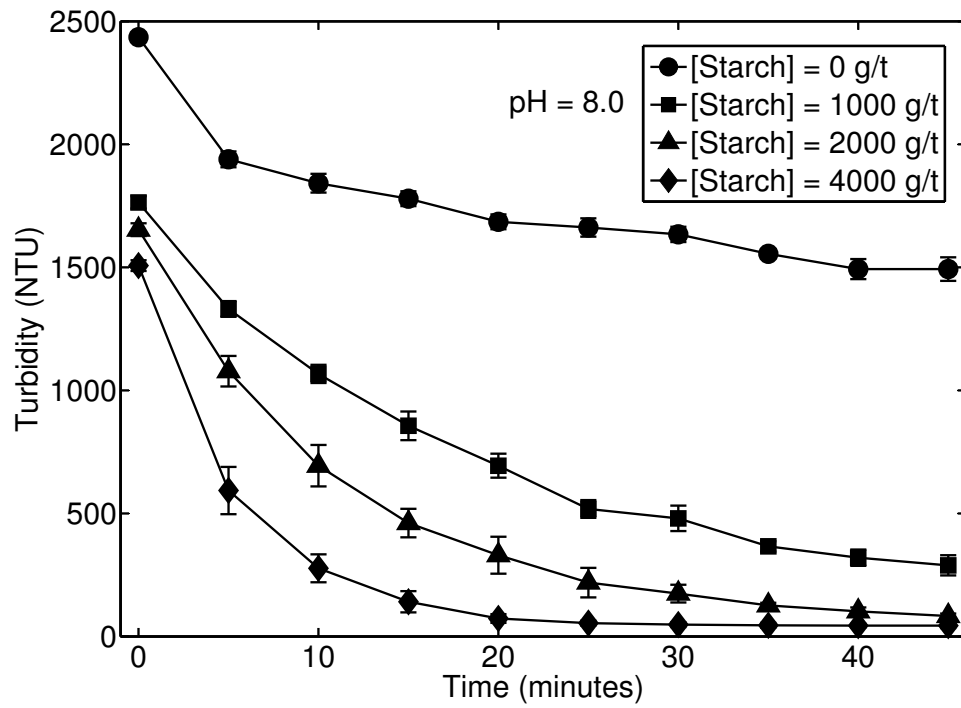
Figure 4.4: Turbidity of crandallite suspension as a function of time in the presence of different concentration of starch at pH 8.0.
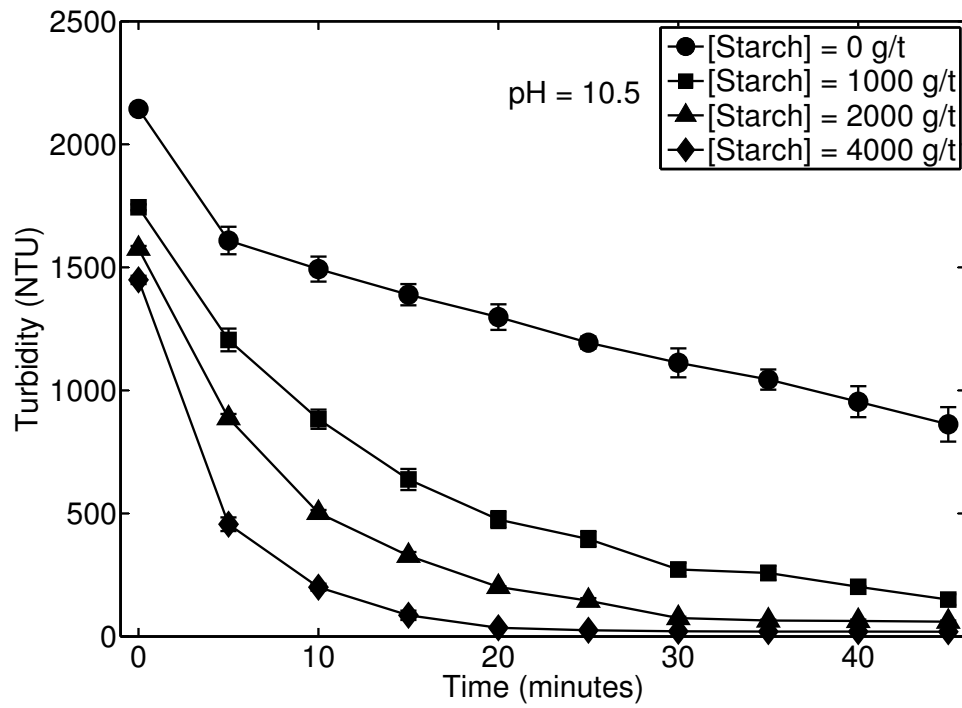
Figure 4.5: Turbidity of crandallite suspension as a function of time in the presence of different concentration of starch at pH 10.5.

performed on fluorapatite and kaolinite by Araujo (1988). He observed that corn starch flocculated fluorapatite extensively, with the highest degree of apatite flocculation observed at pH 10.

Figure 4.4 and Figure 4.5 show the effect of starch at different concentration on the settling kinetics of crandallite at pH values of 8.0 and 10.5, respectively. Starch clearly acts as a flocculant towards crandallite. The fine crandallite particles become unstable when starch is introduced. As starch bridges and flocculates the crandallite particles into flocs, these large aggregates settle quickly leaving a clear supernatant above the sediment. For such a flocculated system, the turbidity of the suspension decreases rapidly and these trends can clearly be seen in Figure 4.4 and Figure 4.5. It is also noteworthy that the results obtained at pH 8 and at pH 10.5 are very similar when one compares the turbidity values for the different starch dosages at a chosen settling time. No evidence of steric re-dispersion was observed in the tested range of starch dosages.

4.4 Effect of Sodium Oleate

Tall oil is used as an anionic collector in phosphate (apatite) flotation at KPO at a pH of 10.5-11.0. Tall oil essentially is a mixture of linoleic and oleic acids, and rosin acids as impurity. Thus it is important to determine its effect on the surface of crandallite, which is treated as a gangue mineral in phosphate flotation. Sun et al. (1957) showed that collecting power of fatty aids for phosphate flotation increases as the degree of unsaturated bonds in the hydrocarbon chains increase until a limit is reached. Thus the following order of collecting power was found for phosphate flotation: linoleic acid >oleic acid >stearic acid. This section deals with the effect of a component of tall oil, oleic acid on the ζ potential and sedimentation properties of crandallite.

Mishra (1978) reported the ζ potential of apatite minerals obtained from different sources. It is interesting to note that the i.e.p. values obtained for different apatite samples were quite different and ranged from 3.5 to 6.7. This was attributed to different impurity contents of the samples. However, the zeta-potential for the apatite samples at higher pH values (at pH >10.0) was found to be similar (close to -20mV).

Mishra (1982) discussed the results on the effect of sodium oleate on

the ζ potential of apatite under constant ionic strength. An large increase in the negative ζ potential, on the order of -20 mV, was observed at pH values greater than i.e.p in the presence of sodium oleate. This change in the ζ potential is a characteristic of some sort of specific adsorption of oleate on the similarly charged surface. However, it was concluded by Mishra (1982) that Coulombic forces were not responsible for such a change in the ζ potential. Chemisorption was proposed as a mechanism of adsorption. Such an increase in the negative ζ potential was also reported by Rao et al. (1990). This negative charge increased with an increase in the concentration of zeta potential above pH 5.0 (Mishra, 1982; Rao et al., 1990).

Mishra (1982) excluded any interaction between phosphate surface and with oleate, but a chemical bond between the calcium species on the surface and oleate was proposed to be the cause of such a change in zeta potential.

At pH 10.0, Rao et al. (1990) showed that the ζ potential of apatite increased with an increase in initial concentration of sodium oleate. This increase was halted when a bilayer formation took place on the surface of apatite. Chemical adsorption on apatite at all pH values was confirmed by Gong et al. (1992) using diffuse reflectance infrared Fourier transform spectroscpy.

Figure 4.6 shows the effect of sodium oleate on the ζ potential of crandallite as a function of pH. The errors in the measurement are equal to the size of the markers used in the figure. An very small increase of about -5mV in negative ζ potential is observed. This increase is equivalent in magnitude to that observed in literature for apatite (Mishra, 1982; Rao et al., 1990). As the mechanism proposed by Rao et al. (1990) and Mishra (1982) involved chemisorption of sodium oleate on the calcium sites on the surface of apatite, it can be concluded that the calcium sites on the surface of crandallite do not favour the same chemisorption of sodium oleate. Thus there seems to be a very limited interaction of sodium oleate with crandallite surface. Therefore, chemisorption can be excluded for being responsible for such a small change in the ζ potential.

Figure 4.7 demonstrates the effect of pH on the turbidity (measured after 45 minutes of observation) of suspension of crandallite (at fixed ionic strength) at various concentrations of oleic acid. Slightly lower turbidity values are observed when oleic acid was introduced in the system. It can
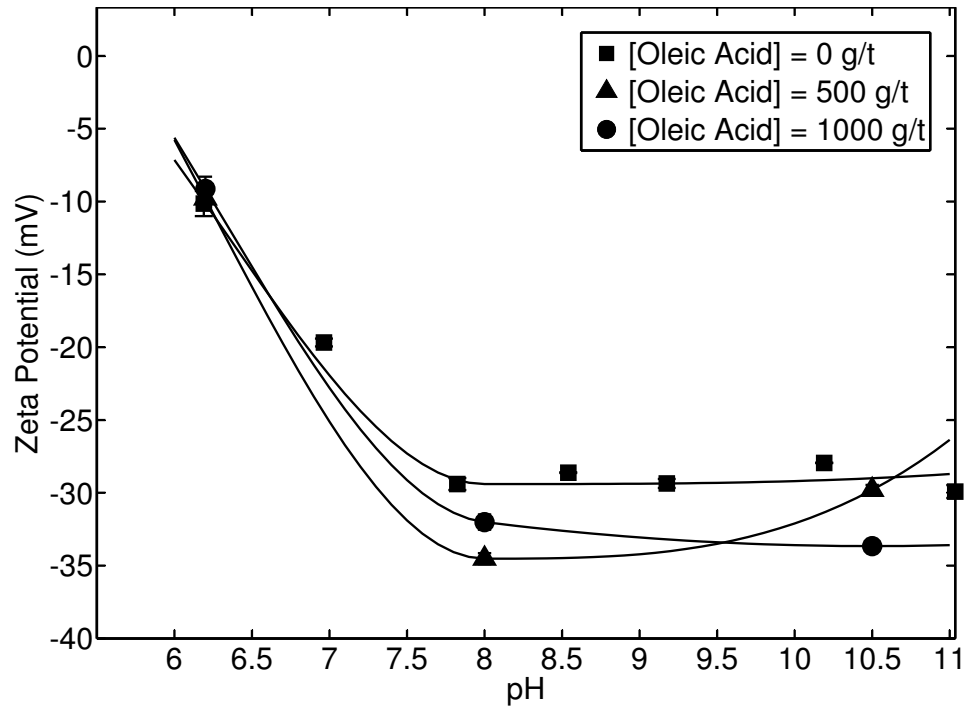
Figure 4.6: Zeta potential of crandallite as a function of pH at different concentrations of oleic acid.
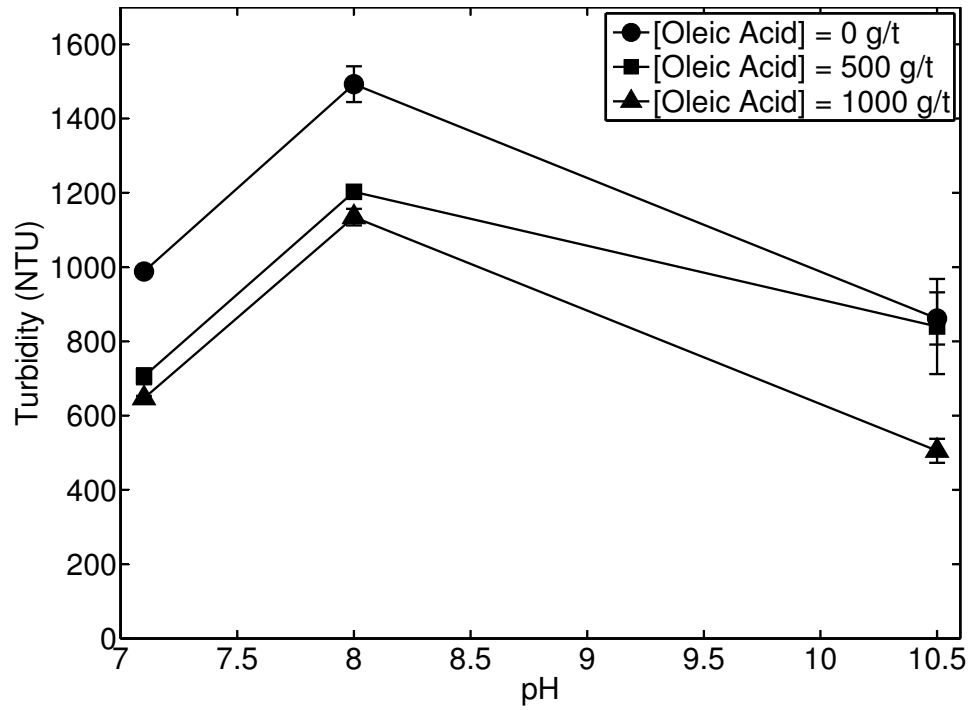
Figure 4.7: Turbidity of crandallite suspension as a function of pH at different concentrations of oleic acid.

also be seen from Figure 4.7 that there is hardly any difference in the turbidity values obtained in the presence of two concentrations (500g/t and 1000g/t).

Just like the zeta potential results, the turbidity results do not provide any indication of strong interactions between the surfactant and the mineral. As there is a very small difference in turbidity values even when the concentration of sodium oleate was doubled, this result further suggests interactions between oleic acid and crandallite are quite different than those between the surfactant and apatite.

4.5 Wettability Study

Contact angle measurements are most often performed on flat polished mineral surfaces to ensure maximum contact between the liquid and the solid. The development of the contact angle is driven by the strength of the adhesion of the liquid to the solid. Weak adhesion results in a high contact angle value and the liquid forms a well define lens/droplet on the solid surface. In contrast, strong adhesion leads to spreading of the liquid on the solid surface producing a very low contact angle value.

In the case of the technique used in this thesis the behavior of water is complicated by the fact that the tested surface is composed of very fine packed particles and as such is highly porous and the development of the contact angle is not so simple to analyze. It should also be recalled that the fine particles that formed the porous layer were first conditioned with an oleic acid solution of known concentration, then the solutions was filtered off, and a droplet of fresh water was finally placed on the filtered bed of particles. This layer most likely still contained a small amount of water. In the course of experiments with fine apatite particles, two types of responses were observed. For low concentrations of oleic acid, when a droplet of water was placed on such a layer, the droplet was instantly absorbed by the layer. For sufficiently high concentrations of oleic acid, a droplet of water placed on the porous layer did not penetrate the layer at all while forming a well defined contact angle on the bed surface. This behavior of water on a porous bed of fine particles is described by the Washburn equation (4.1) (Washburn, 1921). Equation 4.1 with several modifications serves as the basis for many wettability techniques relying on

fine powders (Laskowski, 2001).

$$\frac{l^2}{t} = \frac{\gamma \cos \theta_C}{2\eta} r \qquad (4.1)$$

where r is the uniform internal radius of a single capillary, l is the length of the column of liquid in the capillary at time t, η is the viscosity of the liquid, γ is the surface tension of the liquid, and θ_C is the contact angle.

The depth of penetration, l, can be expected to increase with time, t, but it should be noted that fast and complete penetration is possible only when the cosine of the contact angle is 1 (θ_C=0°). Under these conditions, the penetration rate, defined as l^2/t, reaches a maximum value. For any contact angle larger than 0° the cosine term decreases: it reaches zero for a contact angle of 90°, and decreases to -1 when the contact angle approaches 180°. A contact angle value of more than 90° would result in a negative penetration rate, which physically means that the liquid cannot spontaneously penetrate (or wet) the hydrophobic porous layer, and the measured contact angle results only from adhesion of the liquid to the surface of the bed. For contact angles lower than 90°, some penetration of the bed is possible but after a given time a measurable contact between the liquid and the surface of the bed should still be observed.

Although it is difficult to quantitatively interpret the results, the technique does provide a qualitative answer whether the particles forming the bed are hydrophobic or hydrophilic. Rapid penetration of the bed by water suggests that the particles are hydrophilic while slow or no penetration with a measurable contact angle on the bed surface indicate that the particles are hydrophobic. The reported contact angle values should be treated as qualitative at best, but they can be used to assess the relative wetting behavior of the two minerals.

In the case of fine apatite particles, low dosages of oleic acid do not make the mineral hydrophobic but the contact angle gradually increases at higher concentrations. Indeed, a dosage is reached at which no penetration is observed and the apparent contact angle reaches values on the order of 100°. These results were expected since oleic acid is an excellent collector for apatite and the mineral particles should become hydrophobic after treatment with the surfactant.

Figure 4.8 shows the drop profile on the surface of apatite when conditioned

at an oleic acid concentration of 500g/t and 1000g/t while Figure 4.9 shows the drop profiles at an oleic acid concentration of 2000 g/t and 4000 g/t. Figure 4.10 illustrates the effect of concentration of oleic acid on the measured contact angle for apatite at pH 10.5.

The tests with fine crandallite particles under the same conditions produced quite different results. At pH 10.5, regardless of oleic acid concentration, a droplet of water placed on a bed of crandallite particles wetted the bed completely without developing a finite contact angle. As a result no contact angle could be measured suggesting that the angle under the experimental conditions was actually zero (or very close to zero), and the particles remained hydrophilic even at an oleic acid dosage as high as 4000 g/t. Several tests were also performed at pH 7 at an oleic acid dosage of 2000 g/t, but the result was basically the same as that at pH 10.5. Only rapid and complete wetting of the bed was observed with the apparent contact angle not exceeding 18°.

Overall, no indications of hydrophobicity induced by oleic acid were found for crandallite under the experimental conditions. The results strongly suggest that crandallite particles were not rendered hydrophobic by oleic acid.

The wettability data for crandallite correlate with the zeta potential results that showed only a small effect of oleic acid. At pH 7 and 10.5 the crandallite particles were negatively charged and electrostatic repulsion most likely prevented the adsorption of oleic acid on the mineral particles. This behavior is very different than that of apatite. For apatite, chemical interactions between oleic acid and the mineral render the mineral strongly hydrophobic even at high pH, but in the case of crandallite electrostatic physical interactions appear to be of primary importance.
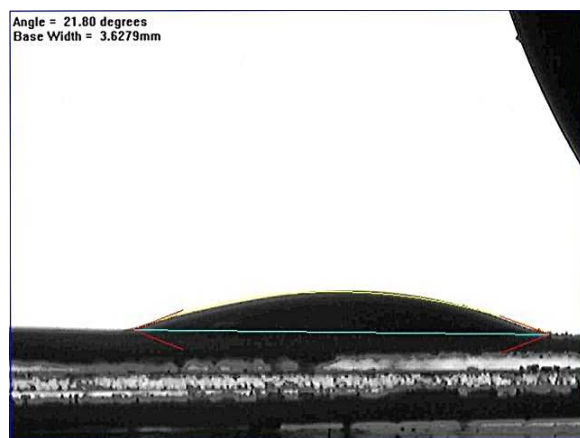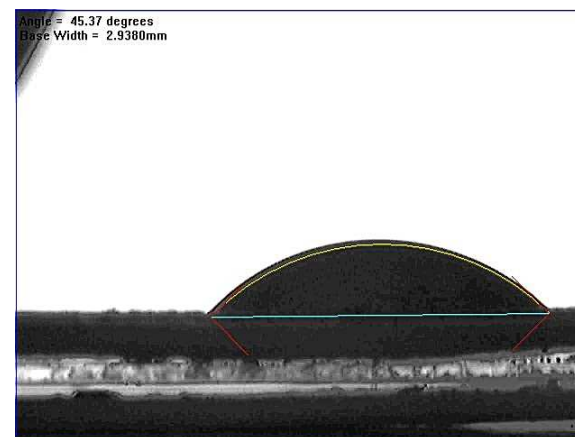
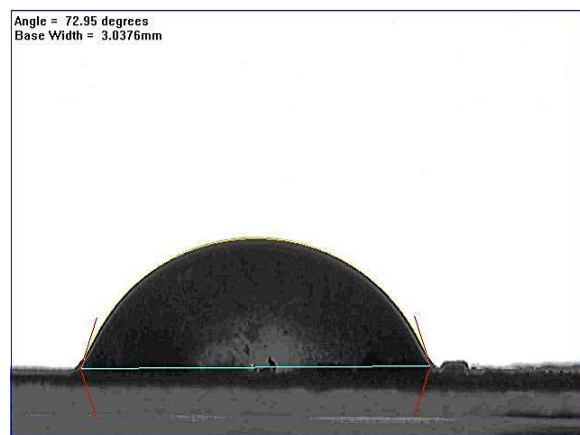**(a)** 500g/t (1).
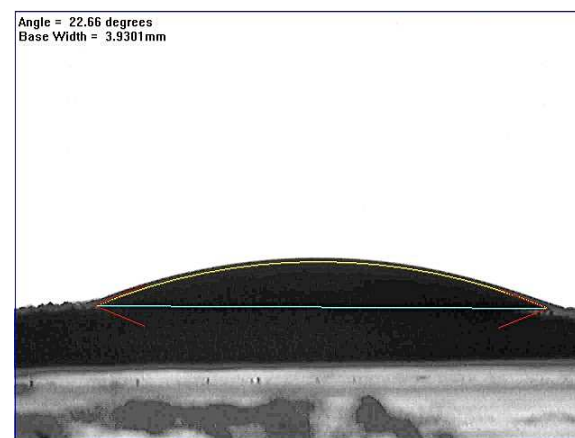
(b) 500g/t (2).
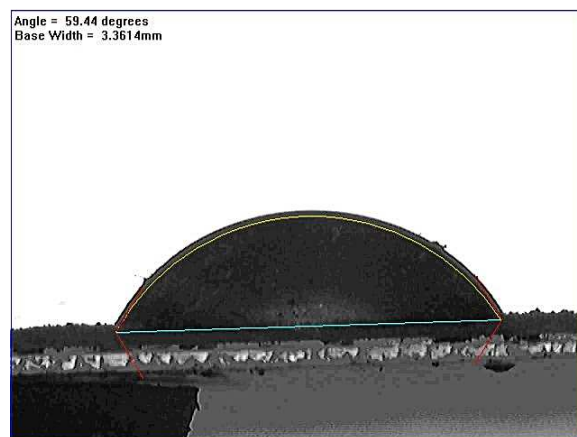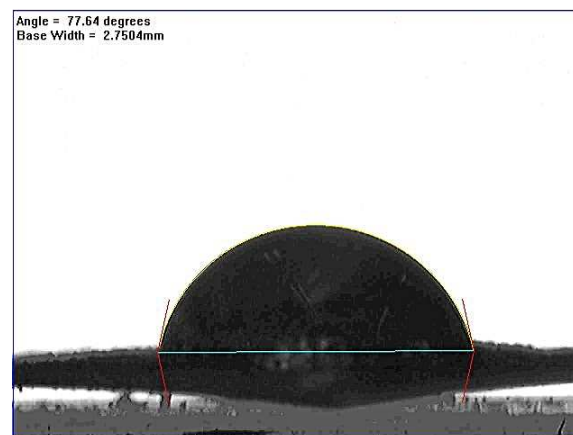
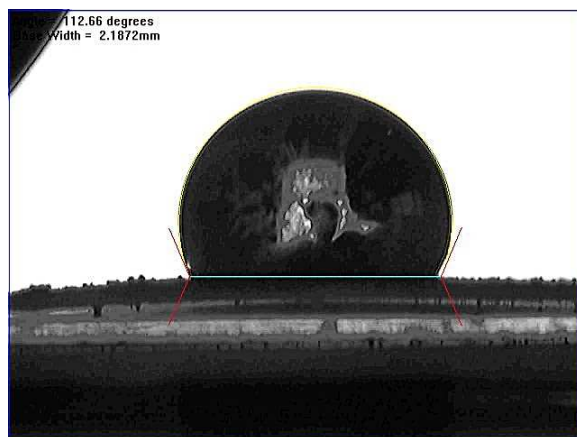**(c)** 1000g/t (1).

(d) 1000g/t (2).

Figure 4.8: Images of water drop on the surface of apatite conditioned at 500g/t and 1000g/t of oleic acid.

(a) 2000g/t (1).

(b) 2000g/t (2).

(c) 3000g/t (1).

(d) 3000g/t (2).

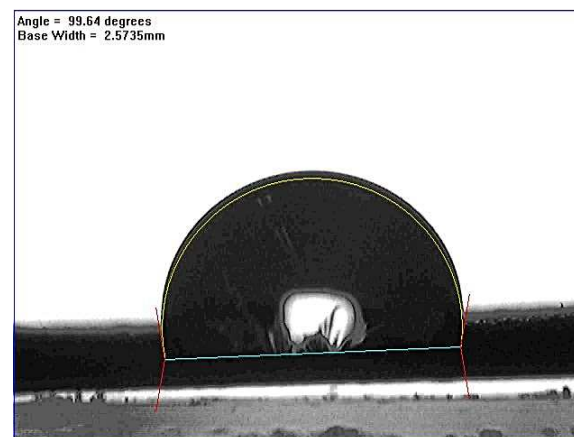**Figure 4.9:** Images of water drop on the surface of apatite conditioned at 2000g/t and 3000g/t of oleic acid.
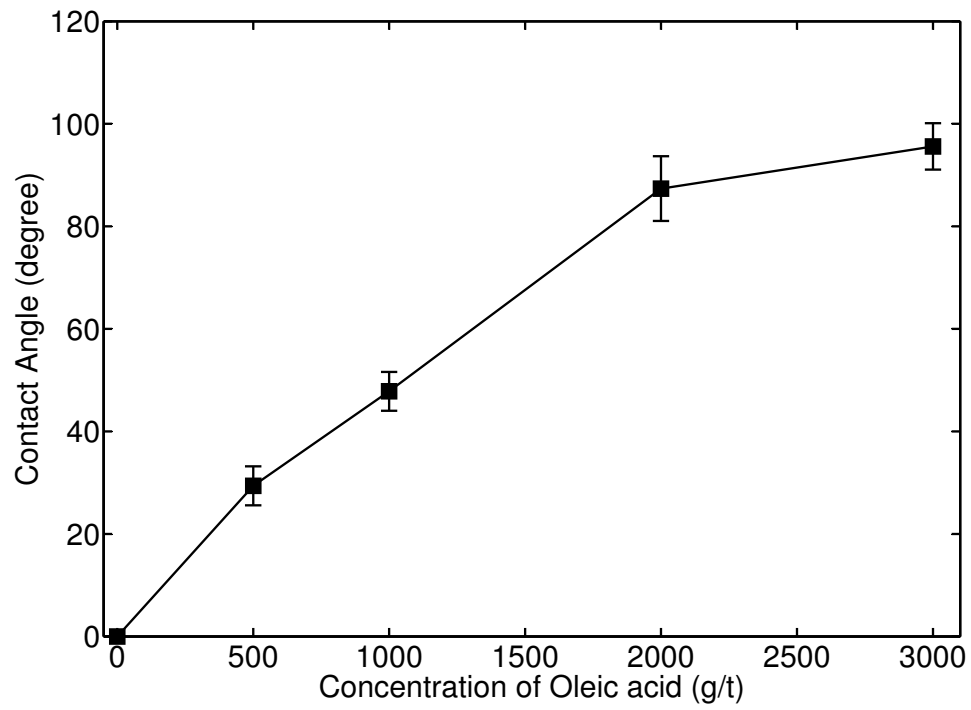
Figure 4.10: Measured contact angle of apatite at different concentrations of oleic acid.

Chapter 5

Conclusion

The electrokinetic results show that in the absence of specifically-adsorbing ions crandallite possesses an iso-electric point at pH 5.5. The effect of calcium ions on the zeta potential of crandallite was two-fold. Calcium acted as a potential determining ion by increasing the iso-electric point to pH 6.3 at a concentration of 75 mg/L. Evidence of specific adsorption of calcium at higher pH was also observed when the zeta potential values approached a second iso-electric point near pH 10. It was generally observed that calcium reduced the magnitude of the zeta potential over the tested pH range.

The electrokinetic results correlated very well with simultaneous stability (turbidity) measurements providing also an indirect confirmation of the measured value of the iso-electric point. The most pronounced aggregation of fine crandallite particles was found to be near pH 5.5-6.0. Under these conditions, or in the absence of electrostatic repulsive forces at the iso-electric point, van der Waals attractive forces dominated the inter-particle force balance leading to aggregation/coagulation of the fine crandallite particles. As a result of the reduction of the magnitude of the zeta potential, the stability of fine crandallite in the presence of calcium was significantly reduced as shown by much lower turbidity values over a wide pH range.

The effect of starch on the turbidity of fine crandallite suspensions was consistent with the flocculant action of the polysaccharide. As the dosage of starch was increased the resulting turbidity values decreased almost to the level of tap water. No signs of steric re-dispersion of crandallite was observed in the tested range of starch dosages. The corresponding changes in the zeta potential values showed only a weak effect of starch which most likely resulted from the non-ionic character of the polymer.

Measurements of the wettability of fine crandallite particles indicated that the mineral particles remained hydrophilic at pH 10.5 and pH 7 for

various dosages of oleic acid. These results suggested that the adsorption of oleic acid on the crandallite particles was driven by physical electrostatic forces rather than by chemical interactions, as in the case of apatite. At the tested pH values the surfaces of the mineral particles were negatively charged and electrostatic repulsion between the particles and the surfactant molecules prevented the adsorption of oleic acid.

These fundamental findings have several important implications for the froth flotation of phosphate ores. It appears that contamination of apatite concentrates by crandallite is primarily caused by the mechanical entrainment of hydrophilic crandallite particles within the apatite concentrate rather than by true flotation of hydrophobic particles. In addition, the use of starch in the froth flotation of apatite ores would provide a means of lowering the extent of mechanical entrainment. Since starch acts as a flocculant towards fine crandallite particles, the flocculated crandallite particles should be less likely to report to the concentrate as they more easily settle compared to dispersed fines.

Chapter 6

Recommendations for Future Work

The presented results were obtained from small scale experiments using very small amounts of available crandallite. Therefore, the majority of suggestions for future research on the subject recommend more detailed investigations with the use of larger samples.

The anionic flotation of crandallite should be tested from either model mixtures of apatite and crandallite or using high-crandallite apatite ores. Aggregation studies between crandallite and apatite mineral should also be carried out in order to identify ranges/domains of interparticle aggregation. Such data would demonstrate the possible carrier flotation phenomena in which fine crandallite particles could potentially report to the concentrate by attachment to coarser apatite particles.

The suggested physical adsorption of oleic acid on the crandallite deserves further research. Direct adsorption measurements of oleic acid on fine crandallite, using much larger amounts of the mineral, should be tested as a function of pH and water chemistry, particularly in the presence of ions such as calcium, magnesium, and sulfates. The anionic flotation of apatite shows seasonal variation in required reagent dosages and in mineral recoveries. In general, the process proceeds faster and more efficiently during summer months so the temperature clearly plays a role. It is plausible that the adsorption of oleic acid and the resulting hydrophobicity and floatability of crandallite also depend on temperature. The adsorption measurements should be supplemented by infrared (FTIR) spectroscopic techniques to identify the adsorption mechanism. Colorimetric measurements of the heat of adsorption would provide further support for the observed mechanisms.

As in the case of apatite, crandallite samples from different sources should be investigated.

Bibliography

S.Z. Abidin, G.K.F. Ling, L.C. Abdullah, S. Ahmad, and T.S.Y. Choong. Effect of temperature and cooling cycles on yield, purity and particle size distribution of dihydroxystearic acid crystals. *European Journal of Scientific Research*, 33(3):471–479, 2009. → pages 29

Abdel-Zahed M. Abouzeid. Physical and thermal treatment of phosphate ores- an overview. *International Journal of Mineral Processing*, 85: 59–84, 2008. → pages 2

J.W. Anthony, R.A. Bideaux, K.W. Bladh, and M.C. Nichols, editors. *Handbook of Mineralogy*, volume IV. Mineral Data Publishing, 2000. → pages 4, 5

A.C. Araujo. *Starch modification of the flocculation and flotation of apatite.* Ph.d. thesis, The University of British Columbia, February 1988. → pages 13, 41, 45

M.T. Beck. Correlation between the "isoelectric point" and stability of complex compounds. *Acta Chim. Acad. Sci. Hung.*, 4:227–230, 1954. → pages 36

F.N. Blanchard. Physical and chemical data for crandallite from Alachua county, Florida. *American Mineralogist*, 57:473–484, 1972. → pages 4, 5

A.M. Blount. The crystal structure of crandallite. *The American Mineralogist*, 59:41–47, 1974. → pages 4, 5

M.D.A Bolland and R.J. Gilkes. How effective are Calciphos and Phospal? *Fertilizer Research*, 12:229–239, 1987. → pages 2

S. Chander, R. Hogg, and D.W. Fuerstenau. Characterization of the wetting and dewetting behavior of powders. *Kona*, 25:56–74, 2007. → pages 32

N.V. Churaev. The relation between colloid stability and wetting. *Journal of Colloid and Interface Science*, 172(2):479 – 484, 1995. → pages 13

H. Cooper, M.C. Fuerstenau, C.C. Harris, M.C. Kuhn, J.D. Miller, and R.F. Yap. *SME Mineral Processing Handbook*, volume 1, pages 1–110. Society of Mining Engineers, New York, NY, 1985. ISBN 0895204336. → pages 41

T. Cosgrove, editor. *Colloid Science: Principles, Methods and Applications*. Blackwell Publishing, 2005. → pages 6, 8, 9, 14, 17

A.V. Delgado, editor. *Interfacial Electrokinetics and Electrophoresis*. Marcel Dekker, Inc., 2002. → pages 6, 17

B.V. Derjaguin and L.D. Landau. Theory of the stability of strongly charged lyophobic sols and the adhesion of strongly charged particles in solutions of electrolytes. *Acta Physicochimica URSS*, 14:633–662, 1941. → pages 12

H.G. Dill. The geology of aluminium phosphates and sulphates of the alunite group minerals: a review. *Earth-Science Reviews*, 53(1-2):35–93, 2001. → pages 4, 20, 23

D. H. Everett. The Royal Society of Chemistry, London, 1988. → pages 12

FAO. Current world fertilizer trends and outlook to 2014. Technical report, Food and Agriculture Organization of the United Nations, 2010. → pages 1

D.W. Fuerstenau and Pradip. Zeta potentials in the flotation of oxide and silicate minerals. *Advances in Colloid and Interface Science*, 114-115: 9–26, 2005. → pages 18

W.Q. Gong, A. Parentich, L.H. Little, and L.J. Warren. Adsorption of oleate on apatite atudied by diffuse reflectance infrared Fourier transform spectroscopy. *Langmuir*, 8:118–124, 1992. → pages 46

S.S. Greenberg and W.T. Elberty. Crandallite (pseudowavellite) from gardner mine ridge, lawrence county, indiana. *The American Mineralogist*, 43(9 & 10):983–985, 1958. → pages 5, 29

R.C. Guimarães, A.C. Araujo, and A.E.C. Peres. Reagents in igenous phosphate ores flotation. *Minerals Engineering*, 18:199–204, 2005. → pages 2, 27, 41

H.C. Hamaker. The London-van der Waals attraction between spherical particles. *Physica*, 4(10):1058–1072, 1937. → pages 9

D.C. Henry. The cataphoresis of suspended particles. Part I. the equation of cataphoresis. *Proc. R. Soc. Lond. A*, 133:106–129, 1931. → pages 17

P. Hoffmann, I. Schmidtke, and K.H. Lieser. Speciation of phosphates in aqueous solutions by ion chromatography. *Fresenius' Journal of Analytical Chemistry*, 335(4):402–403, 1989. → pages 7

E. Hückel. Die kataphoresese der kugel. *Physikalische Zeitschrift*, 25: 204–210, 1924. → pages 17

R.J. Hunter. *Foundations of Colloid Science.* Clarendon Press, Oxford, 1987. → pages 12

R.J. Hunter. *Introduction to modern colloid science.* Oxford University Press Inc., New York, 1st edition, 1993. → pages 10, 13, 14, 15, 17, 18

R. O. James and T. W. Healy. Adsorption of hydrolysable metal ions at the oxide-water interface, Part I, II and III. *Journal of Colloid and Interface Science*, 40:42–52, 53–64, 65–81, 1972. → pages 40

J.S. Laskowski, editor. *Coal Flotation and Fine Coal Utilization.* Elsevier, 2001. → pages 50

G.F. Loughlin and W.T. Schaller. Crandallite, a new mineral. *American Journal of Science*, 43(253):69–74, 1917. → pages 4, 5

S.J. Mills, F. Hatert, E.H. Nickel, and G. Ferraris. The standardisation of mineral group hierarchies: application to recent nomenclature proposals. *European Journal of Mineralogy*, 21:1073–1080, 2009. → pages 4

S.K. Mishra. The electrokinetics of apatite and calcite in inorganic electrolyte environment. *International Journal of Mineral Processing*, 5: 69–83, 1978. → pages 45

S.K. Mishra. Electrokinetic properties and flotation behaviour of apatite and calcite in the presence of sodium oleate and sodium metasilicate. *International Journal of Mineral Processing*, 9:59–73, 1982. → pages 45, 46

E. Mularczyk and J. Drzymala. Removal of decomposition products from sodium oleate. *Industrial and Engineering Chemistry Research*, 35: 788–791, 1996. → pages 27

B. Nanthakumar, D. Grimm, and M. Pawlik. Anionic flotation of high-iron phosphate ores- Control of process water chemistry and depressrion of iron minerals by starch and guar gum. *International Journal of Mineral Processing*, 92:49–57, 2009. → pages 23

Donald H. Napper. *Polymeric stabilization of colloidal dispersions.* Academic Press, New York, 1983. → pages 14

A.S. Peck and M.E. Wadsworth. Infrared studies of oleic acid and sodium oleate adsorption on fluorite, barite and calcite. Report of Investigations 6202, US Bureau of Mines, 1963. → pages 2

A.S. Peck and M.E. Wadsworth. IR studies of the effect of F^-, SO_4^{-2}, and Cl^- ions on the chemisorption of oleate on fluorite, barite and calcite. In N. Arbiter, editor, *Processings of the 7-th International Mineral Processing Congress*, pages 259–267. Gordon and Breach, New York, 1965. → pages 2

O.S. Pokrovsky, J.A. Mielczarski, O. Barres, and J. Schott. Surface speciation models of calcite and dolomite/aqueous solution interfaces and their spectroscopic evaluation. *Langmuir*, 16:2677–2688, 2000. → pages 8

K.H. Rao, B-M. Antti, and E. Forssberg. Mechanism of oleate interaction on salt-type minerals, Part II. adsorption and electrokinetic studies of apatite in the presence of sodium oleate and sodium metasilicate. *International Journal of Mineral Processing*, 28:59–79, 1990. → pages 46

B. Salopek, D. Krasic, and S. Filipovic. Measurement and application of zeta-potential. *Rudarsko-Geolosko-Naftni Zbornik*, 4:147–151, 1992. → pages 5, 18, 19

H. Sis and S. Chander. Reagents used in the flotation of phosphate ores: a critical review. *Minerals Engineering*, 16:577–585, 2003. → pages 2, 41

B. Siwek, M. Zembala, and A. Pomianowski. A method of determination of fine particle flotability. *International Journal of Mineral Processing*, 8:85–88, 1981. → pages 32

P. Somasundaran. Zeta potential of apatite in aqueous solutions and its change during equilibrium. *Journal of Colloid and Interface Science*, 27 (4):659–666, 1968. → pages 36

S.C. Sun, R.E. Snow, and V.I. Purcell. Flotation characteristics of a Florida Leached Zone phosphate ore with fatty acids. *Transaction of the American Institute of Mining, Metallurgical and Petroleum Engineers*, 208:70–75, 1957. → pages 45

Th.F. Tadros. Control of properties of suspensions. *Colloids and Surfaces*, 18:137–173, 1986. → pages 12

UNIDO and IFDC. *Fertilizer Manual.* United Nations Industrial Development Organization (UNIDO) and International Fertilizer Development Center (IFDC), 3rd edition, 1998. → pages 1, 2

E.J.W. Verwey and J.T.G. Overbeek. *The Stability of Lyophobic Colloids.* Elsevier, Amsterdam, 1948. → pages 12

Edward W. Washburn. The dynamics of capillary flow. *Phys. Rev.*, 17: 273–283, 1921. → pages 49

Appendix A

Rietveld Refinement Plots
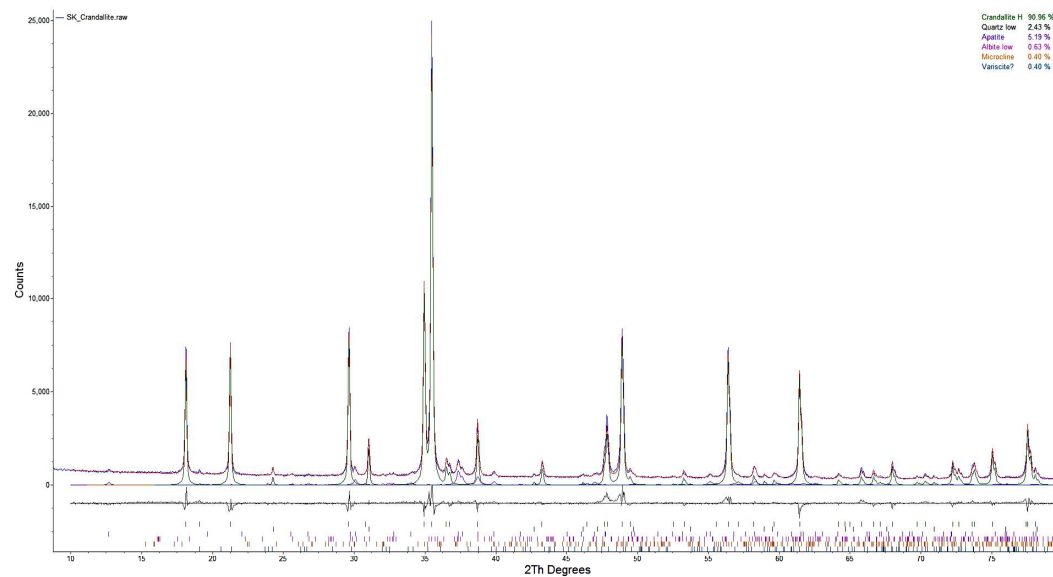
Figure A.1: Rietveld refinement plot of crandallite(blue line - observed intensity at each step; red line - calculated pattern; solid grey line below difference between observed and calculated intensities; vertical bars, positions of all Bragg reflections). Coloured lines are individual diffraction patterns of all phases.
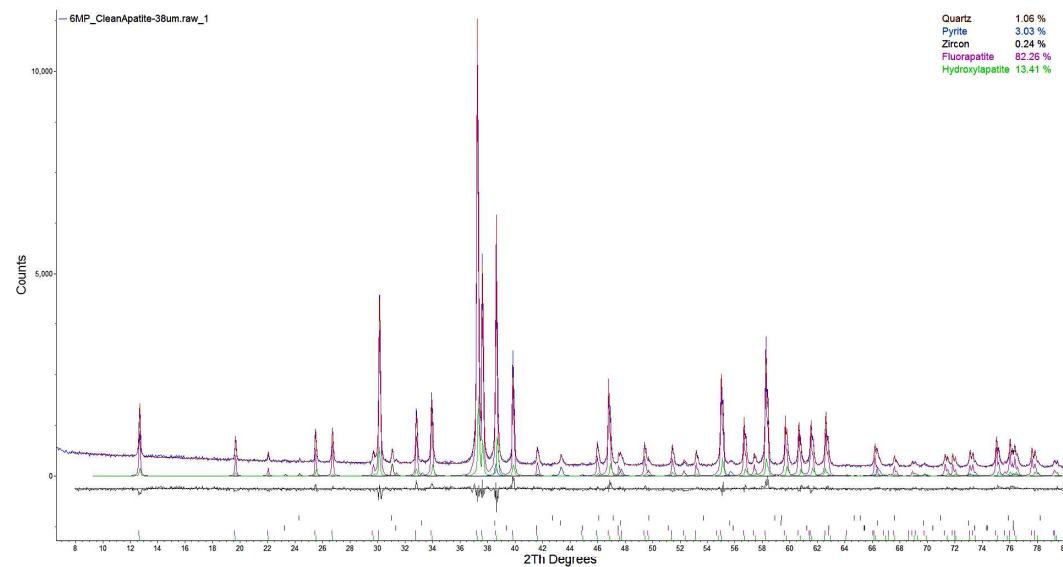
Figure A.2: Rietveld refinement plot of apatite(blue line - observed intensity at each step; red line - calculated pattern; solid grey line below difference between observed and calculated intensities; vertical bars, positions of all Bragg reflections). Coloured lines are individual diffraction patterns of all phases.
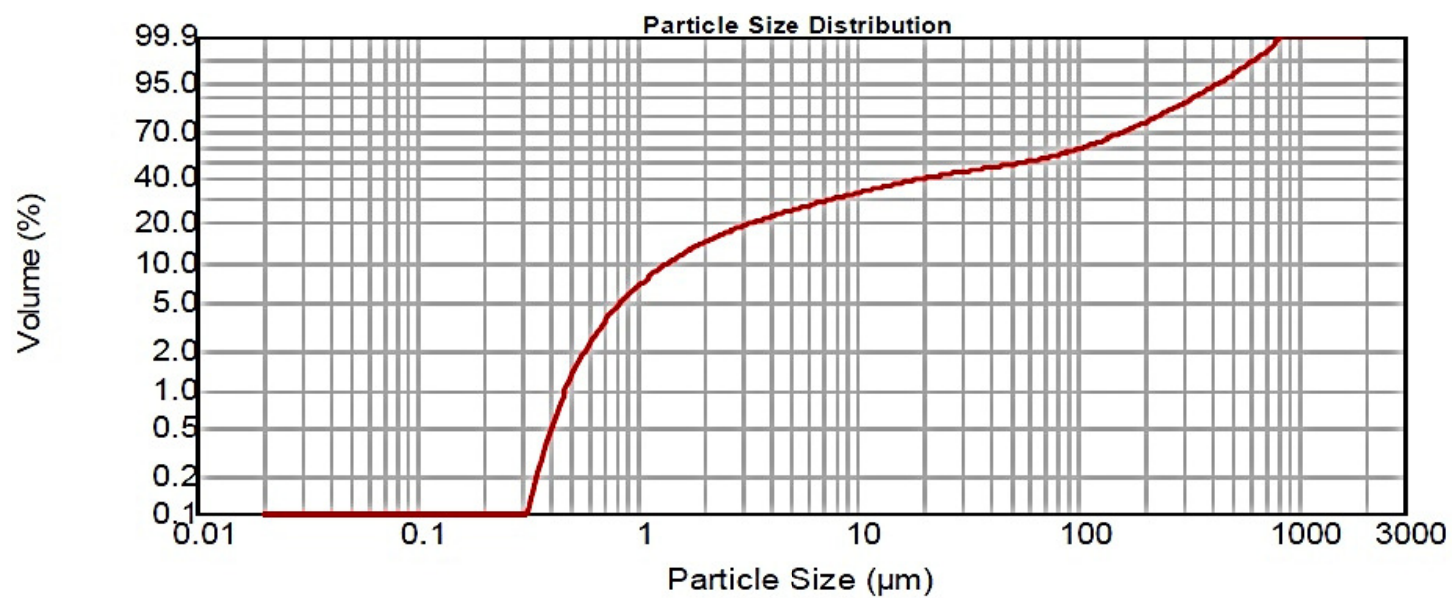
Appendix B

Particle Size Analysis: Rosin-Rammler Plots

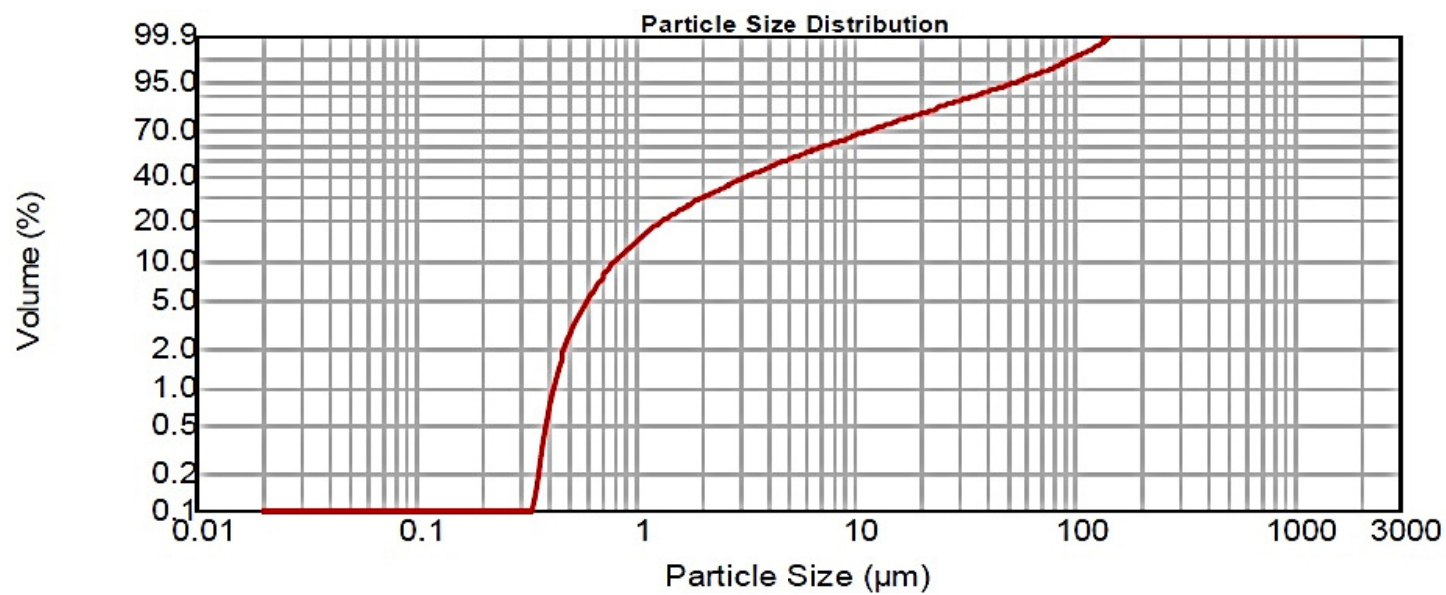**Figure B.1:** Rosin-Rammler plot of crandallite sample after being dry pulverized in a ceramic mill.

Figure B.2: Rosin-Rammler plot of crandallite sample after being dry pulverized in a SPEX mill for two minutes.
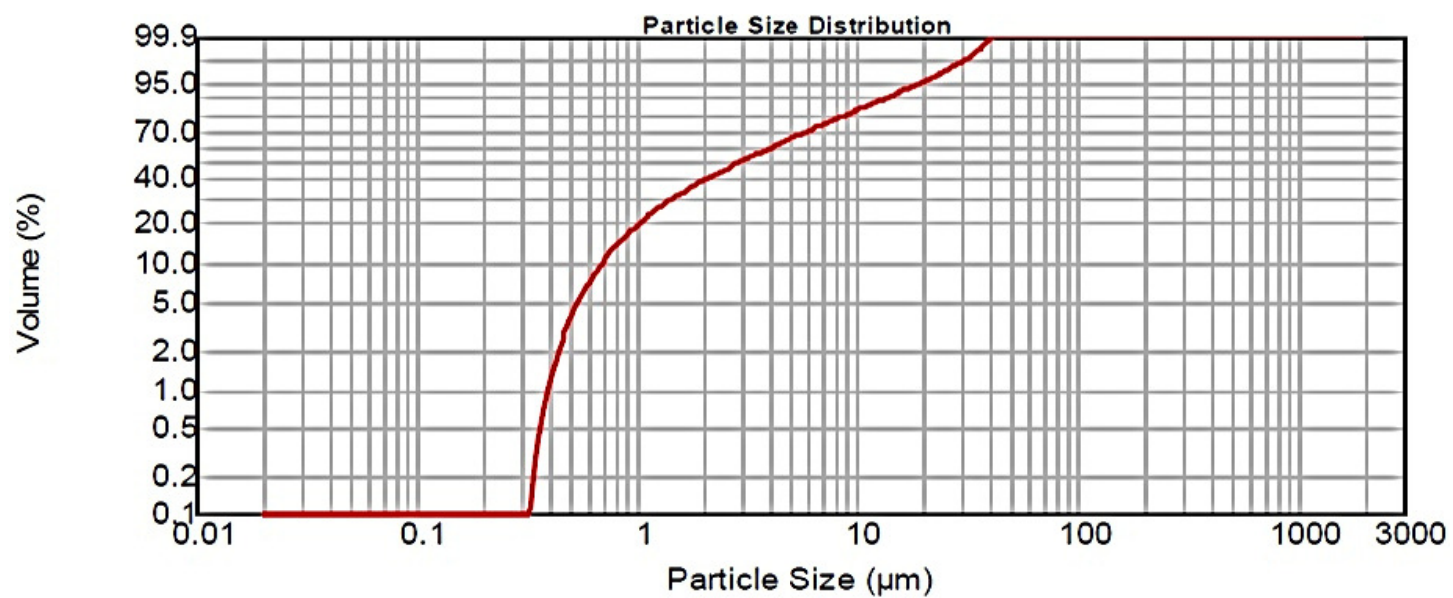
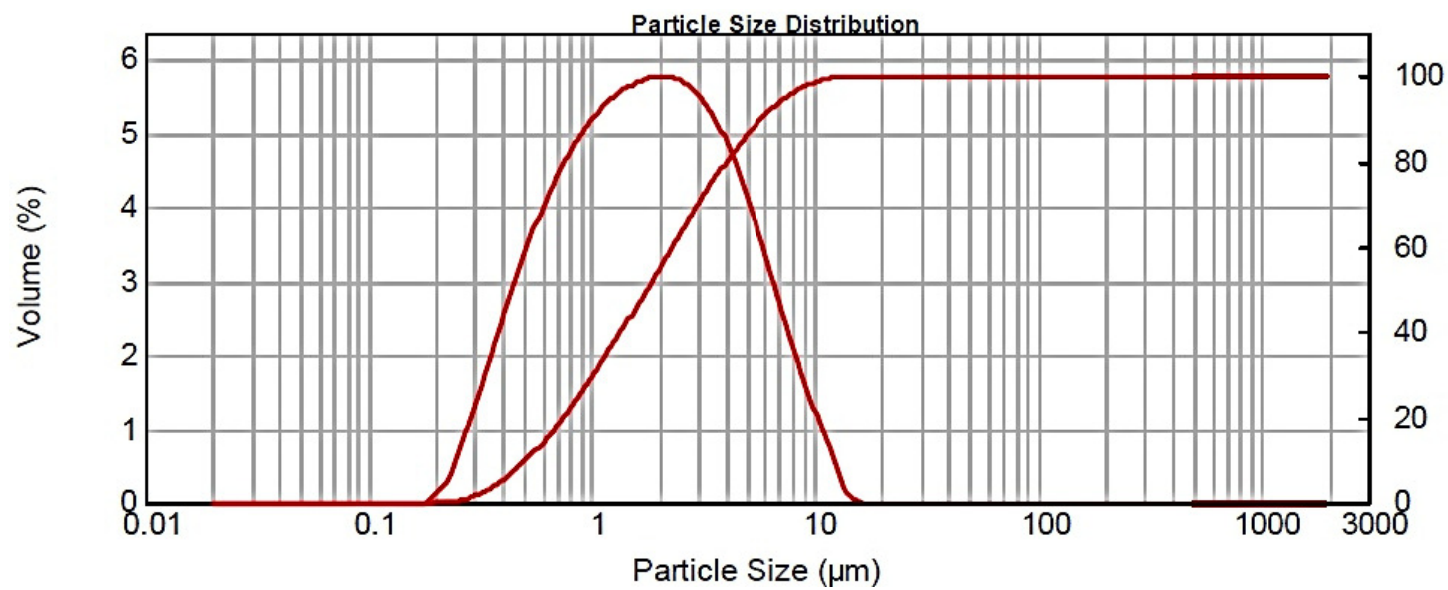**Figure B.3:** Rosin-Rammler plot of crandallite sample after being dry pulverized in a SPEX mill for seven minutes.

Figure B.4: Rosin-Rammler plot of apatite sample after being dry pulverized in a SPEX mill for three minutes.
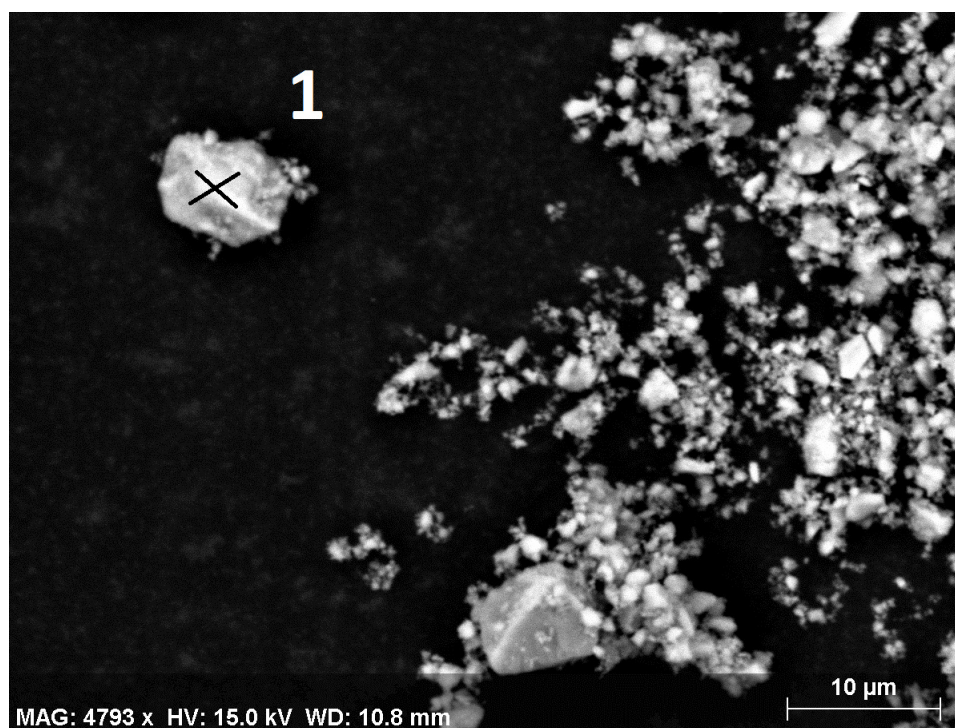
Appendix C

SEM-EDX Plots

Figure C.1: Crandallite 1 picture for EDX analysis. The 'X' on the picture mark the particle in the picture which was analyzed by EDX and for which the EDX spectra is mentioned.

MAG: 2397 x HV: 15.0 kV WD: 10.8 mm

20 µm

2

Figure C.2: Crandallite 2 picture for EDX analysis. The 'X' on the picture mark the particle in the picture which was analyzed by EDX and for which the EDX spectra is mentioned.
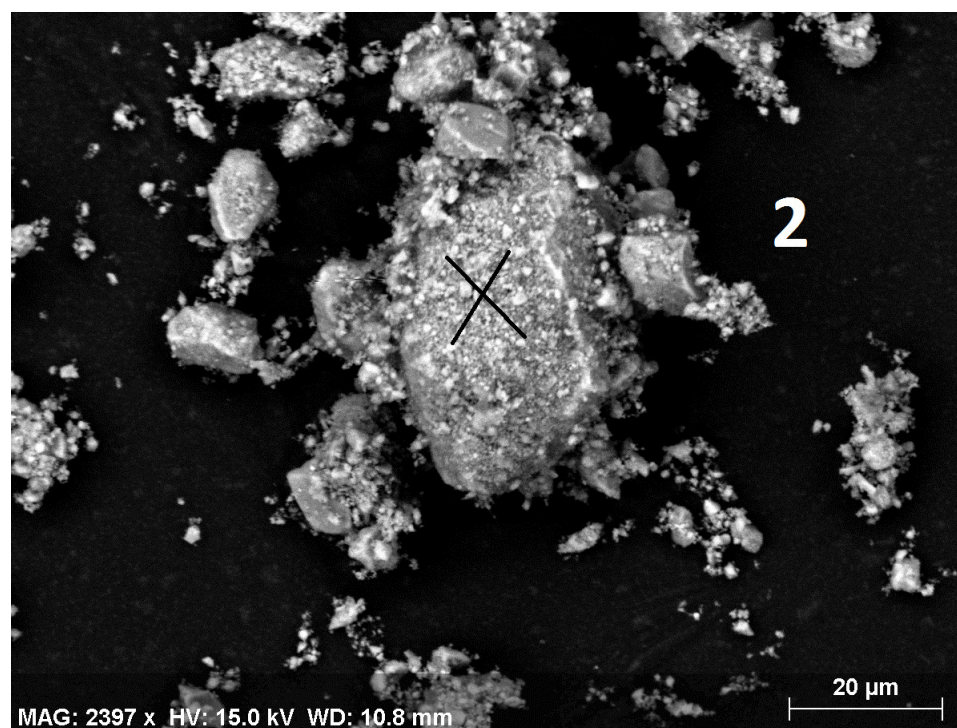
Figure C.3: Apatite 1 and Apatite 2 picture for EDX analysis. The 'X' on the picture mark the particle in the picture which was analyzed by EDX and for which the EDX spectra is mentioned.
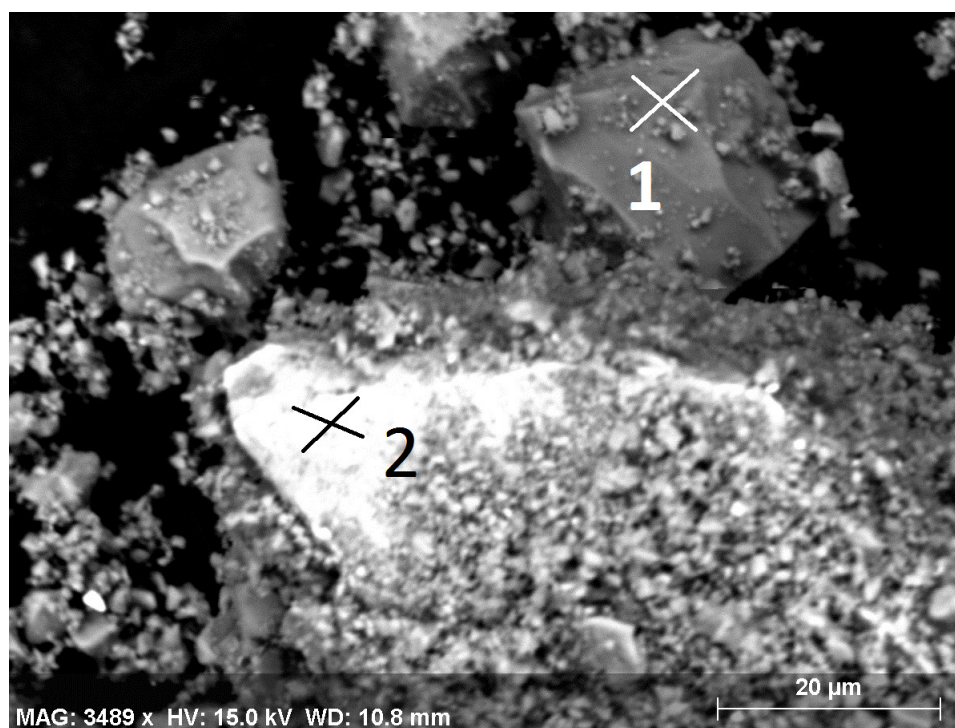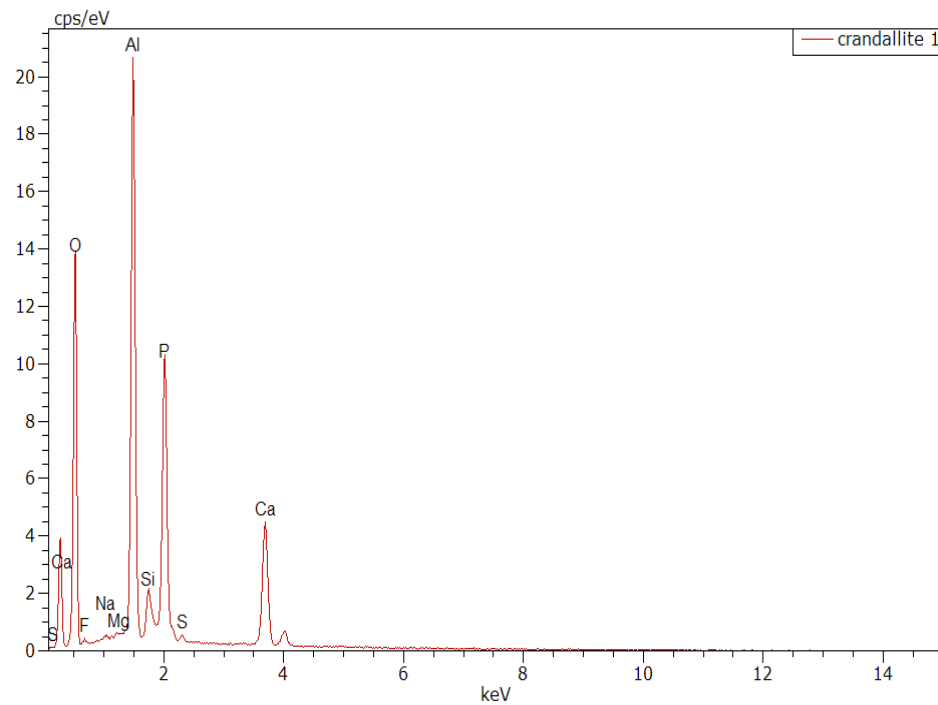
Figure C.4: EDX spectra for Figure C.1. The peak analysis analysis of EDX spectra shows that the mineral might be crandallite when it is compared with its chemical formaula.
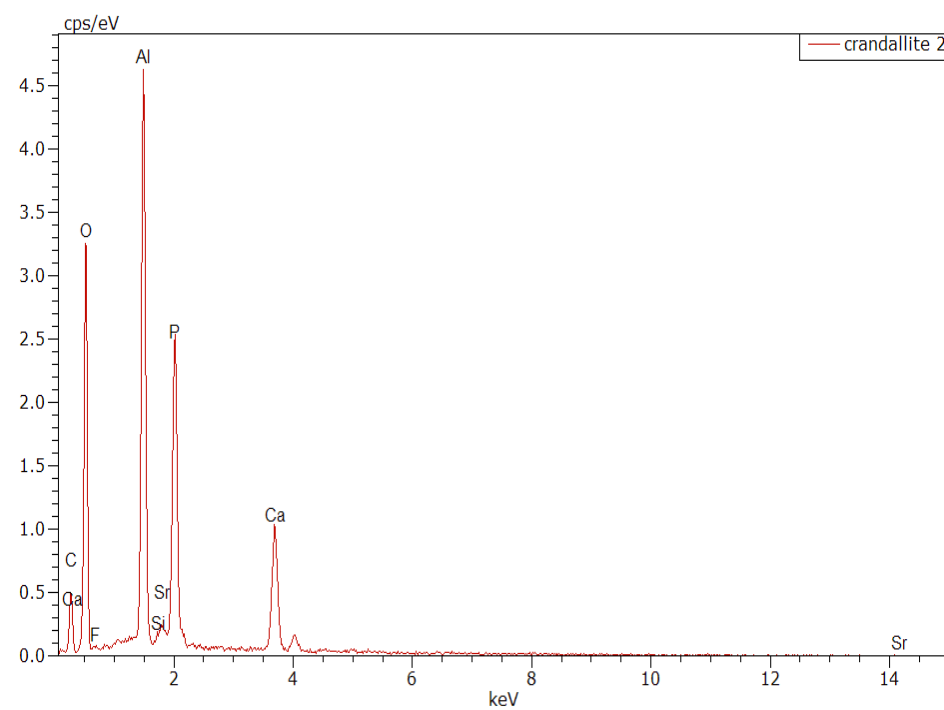
Figure C.5: EDX spectra for Figure C.2. The peak analysis analysis of EDX spectra shows that the mineral might be crandallite when it is compared with its chemical formaula. There might be a possibility of lattice substitution by Strontium.

Figure C.6: EDX spectra for Figure C.3. The peak analysis analysis of EDX spectra shows that the mineral might be apatite when it is compared with its chemical formaula.

Figure C.7: EDX spectra for Figure C.3. The peak analysis analysis of EDX spectra shows that the mineral might be pyrite when it is compared with its chemical formaula. There is some evidence of pyrtie in the sample from the XRD analysis of apatite sample (Table 3.2).
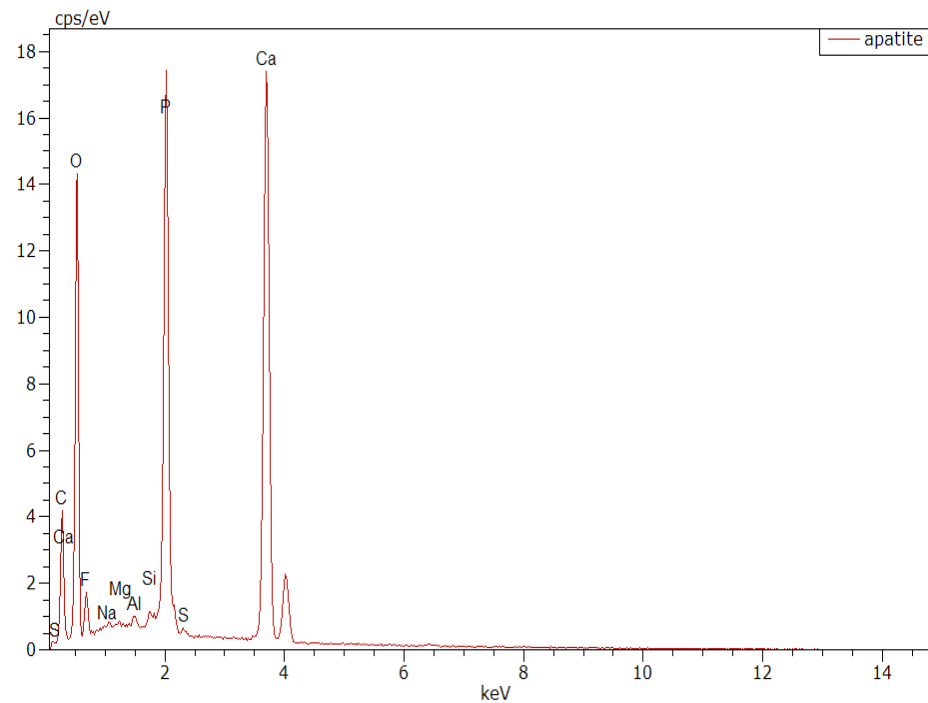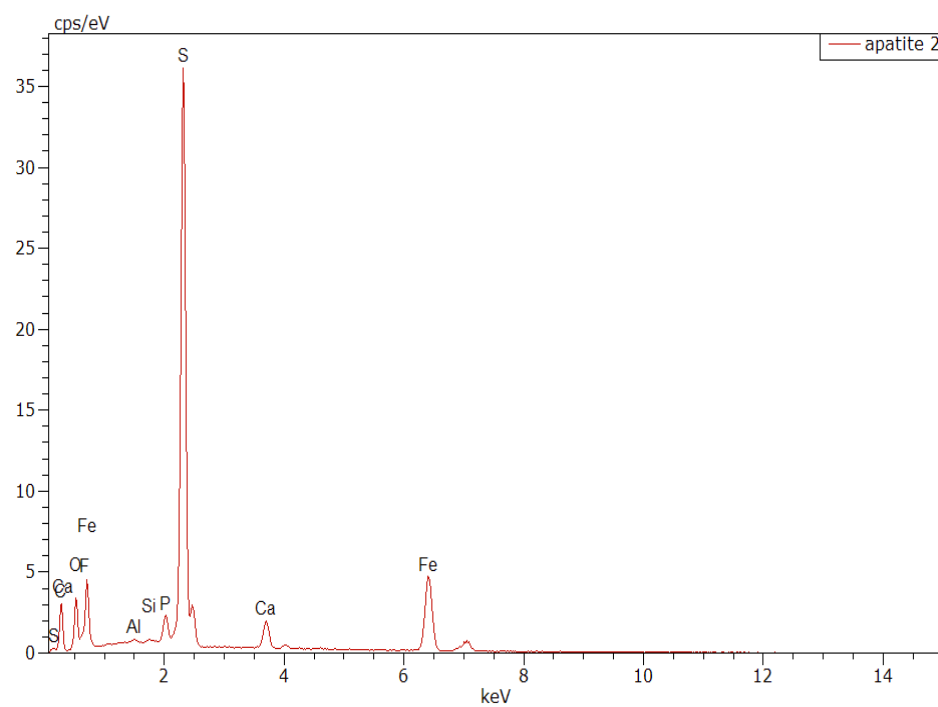
Appendix D

Eleven-point BET Analysis Plots

Figure D.1: Quantachrome Autosorb Automated Gas Sorption System Report- BET Plot for crandallite.

05/22/2012

Quantachrome Instruments
Quantachrome Autosorb Automated Gas Sorption System Report
Autosorb 1 for Windows 1.52

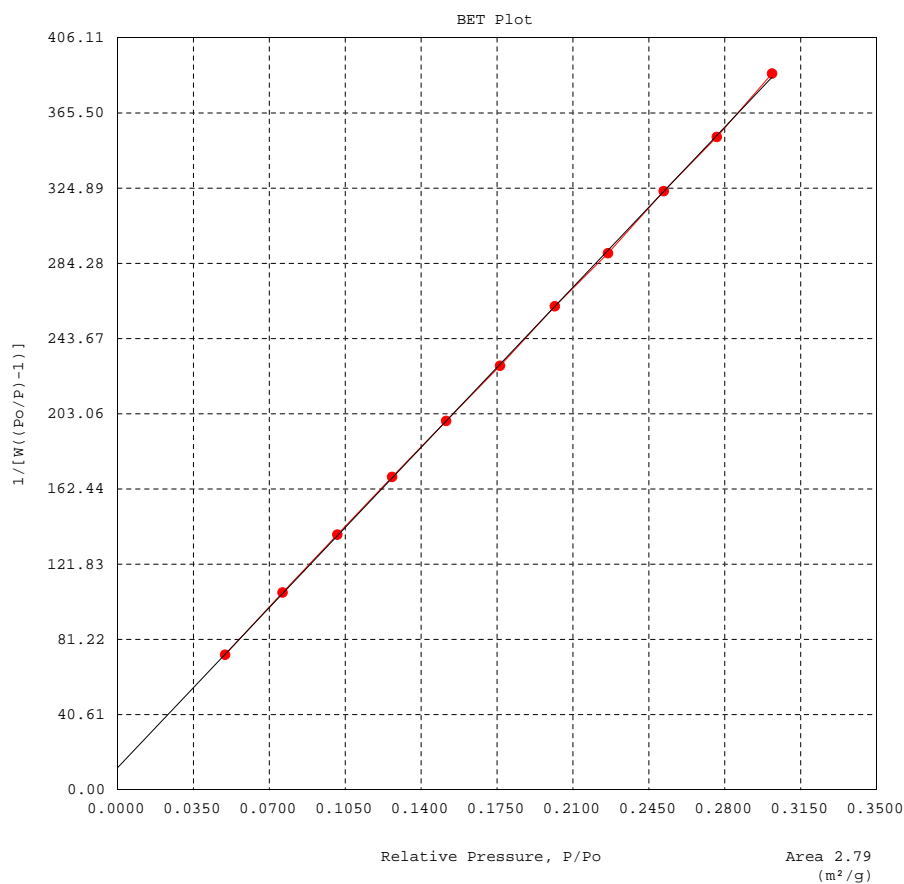|					
File name:	C:\QCdata\PhysData\Sarthak\Apatite.raw				
Sample ID:	AS_20120514_1	**Description:**	Apatite		
Comments:					
Operator:	Sarthak	**Sample weight:**	0.9761 g		
Analysis gas:	Nitrogen	**X sect. area:**	16.2 Å²/molec	**Non-ideality:**	6.58e-05
Adsbate (DRP):	Nitrogen	**Bath Temp.:**	77.30		
Outgas Temp:	300.0 ºC	**Outgas Time:**	1.0 hrs	**Analysis Time:**	74.8 min
P/Po tolerance:	0	**Equil. time:**	3	**End of run:**	05/14/2012 15:40
Station #:	1	**PC sw. version:**	1.52	**TempComp:**	On

A —●— BF ———

Figure D.2: Quantachrome Autosorb Automated Gas Sorption System Report- BET Plot for apatite.

81

Appendix E

ParticleMetrix Report of Zeta potential

ZETAVIEW® Laser Scattering Video Microscope
PARTICLEMETRIX www.particle-metrix.de

Electrophoresis & Brownian Motion
Video Analysis
Laser Scattering Microscopy

Operator (Report): zeta
Video Operator: zeta

Sample Parameters
Sample Name: Crandallite
Comment: Sample Checked: 2011-10-24 18:20:40
SL1 OK: OK, SL2 OK: OK, Number of Good Positions: 11
Electrolyte: NaCl, Concentration: 0.010 N
Temperature: 26.17 °C sensed
pH 5.0 entered
Conductivity: 1159.09 µS/cm sensed

Measurement Parameters
Cell S/N: 1141x10_Z157
Sensed Electric Field: 3.59 V/cm
Measurement Mode: Stationary 8 Cycles

Result
Mobility: 0.33 FWHM 0.78 µm/sec/V/cm, @ 25°C: 0.32 µm/sec/V/cm
ZP Factor 12.6 (Smoluchowski):
Zeta Potential @ 25 °C: 4.11 FWHM 9.77 mV

Quality
Number of Traced Particles: 362
ΔSL: 6.76 mV

Analysis Parameters
Max Size: 100, Min Size: 10, Min Brightness: 20

Stationary Layers	Rel. Position
SL1	0.149
SL2	0.851

Peak Analysis (25 °C)

Zeta Potential / mV	Frequency	FWHM / mV	Percentage
5.2752	0.8118	10.3987	100.0000

Comment

(Signature)

Analyzed Video: C:\Users\zeta\Documents\ZetaData157UBC4Sept2011\20111024_0011_Cran 8bi_SL_comp.avi

ZetaVIEW S/N 157, Software ZetaView 8.01.03, Camera 0.703 µm/px

Experiment: October-24-11 18:23, Report: 2011-10-24 18:29

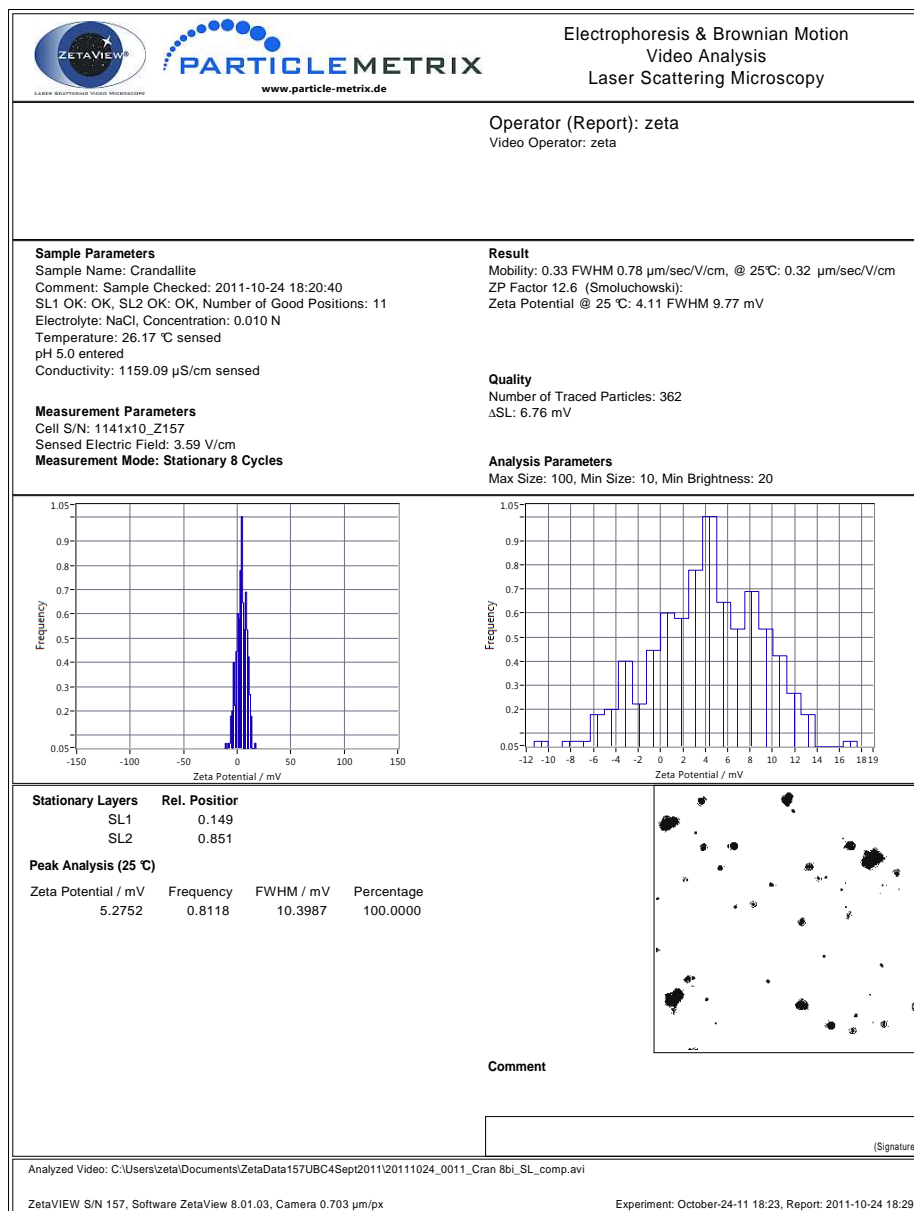**Figure E.1:** Electrophoresis and brownian motion video analysis report generated by ZetaView®.